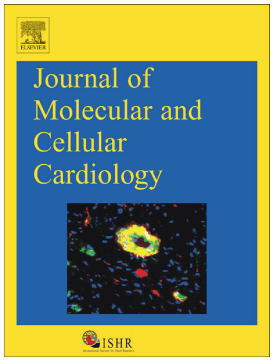

InsP3R-RyR channel crosstalk augments sarcoplasmic reticulum Ca2+ release and arrhythmogenic activity in post-MI pig cardiomyocytes

Xin Jin, Anna Meletiou, Joshua Chung, Agne Tilunaite, Kateryna Demydenko, Eef Dries, Rosa Doñate Puertas, Matthew Amoni, Ashutosh Tomar, Piet Claus, Christian Soeller, Vijay Rajagopal, Karin Sipido, H. Llewelyn Roderick

PII: S0022-2828(23)00062-7

DOI: https://doi.org/10.1016/j.yjmcc.2023.03.015

Reference: YJMCC 9636

To appear in: *Journal of Molecular and Cellular Cardiology*

Received date: 17 November 2022

Revised date: 8 March 2023

Accepted date: 28 March 2023

Please cite this article as: X. Jin, A. Meletiou, J. Chung, et al., InsP3R-RyR channel crosstalk augments sarcoplasmic reticulum Ca2+ release and arrhythmogenic activity in post-MI pig cardiomyocytes, *Journal of Molecular and Cellular Cardiology* (2023), https://doi.org/10.1016/j.yjmcc.2023.03.015

$InsP_3R$-RyR channel crosstalk augments sarcoplasmic reticulum Ca^{2+} release and arrhythmogenic activity in post-MI pig cardiomyocytes

Xin Jin[1,&], Anna Meletiou[2$], Joshua Chung[1,3$], Agne Tilunaite[3,4], Kateryna Demydenko[1], Eef Dries[1], Rosa Doñate Puertas[1], Matthew Amoni[1], Ashutosh Tomar[1], Piet Claus[1], Christian Soeller[2], Vijay Rajagopal[3], Karin Sipido[1] and H. Llewelyn Roderick[1*]

[1]KU Leuven, Department of Cardiovascular Sciences, Laboratory of Experimental Cardiology, B-3000, Leuven.

[2]Department of Physiology, University of Bern, Bern, Switzerland

[3]Cell Structure and Mechanobiology Group, Department of Biomedical Engineering, Melbourne School of Engineering, University of Melbourne, Australia.

[4]Systems Biology Laboratory, School of Mathematics and Statistics, and Department of Biomedical Engineering, University of Melbourne, Australia.

[$]equal contribution as second authors.

*For correspondence: Llewelyn.roderick@kuleuven.be

[&]Current address: Department of Internal Medicine, Carver College of Medicine, University of Iowa, Iowa City, Iowa, United States of America.

Abstract

Ca^{2+} transients (CaT) underlying cardiomyocyte (CM) contraction require efficient Ca^{2+} coupling between sarcolemmal Ca^{2+} channels and sarcoplasmic reticulum (SR) ryanodine receptor Ca^{2+} channels (RyR) for their generation; reduced coupling in disease contributes to diminished CaT and arrhythmogenic Ca^{2+} events. SR Ca^{2+} release also occurs via inositol

1,4,5-trisphosphate receptors ($InsP_3R$) in CM. While this pathway contributes negligeably to Ca^{2+} handling in healthy CM, rodent studies support a role in altered Ca^{2+} dynamics and arrhythmogenic Ca^{2+} release involving $InsP_3R$ crosstalk with RyRs in disease. Whether this mechanism persists in larger mammals with lower T-tubular density and coupling of RyRs is not fully resolved. We have recently shown an arrhythmogenic action of $InsP_3$-induced Ca^{2+} release (IICR) in end stage human heart failure, often associated with underlying ischemic heart disease (IHD). How IICR contributes to early stages of disease is however not determined but highly relevant. To access this stage, we chose a porcine model of IHD, which shows substantial remodelling of the area adjacent to the infarct. In cells from this region, IICR preferentially augmented Ca^{2+} release from non-coupled RyR clusters that otherwise showed delayed activation during the CaT. IICR in turn synchronised Ca^{2+} release during the CaT but also induced arrhythmogenic delayed afterdepolarizations and action potentials. Nanoscale imaging identified co-clustering of $InsP_3Rs$ and RyRs, thereby allowing Ca^{2+}-mediated channel crosstalk. Mathematical modelling supported and further delineated this mechanism of enhanced $InsP_3R$-RyRs coupling in MI. Our findings highlight the role of $InsP_3R$-RyR channel crosstalk in Ca^{2+} release and arrhythmia during post-MI remodelling.

Keywords:

Ischemic heart disease; myocardial infarction; Excitation contraction coupling; cardiac arrhythmia; Ca^{2+} homeostasis, inositol 1,4,5-trisphosphate receptor.

Abbreviations:

Excitation contraction coupling (ECC), action potential (AP), delayed after depolarisation (DAD), inositol 1,4,5-trisphosphate ($InsP_3$), $InsP_3$ receptor ($InsP_3R$), $InsP_3$-induced Ca^{2+} release (IICR), cardiomyocyte (CM), myocardial infarction (MI), sarcoplasmic reticulum (SR), L-type Ca^{2+} channel (LTCC), ryanodine receptor (RyR), sarco/endoplasmic reticulum Ca^{2+} ATPase (SERCA), calsequestrin (CSQ), sodium/calcium (Na^+/Ca^{2+}) exchanger (NCX), Ca^{2+} calmodulin kinase II (CaMKII), Ca^{2+} transient (CaT), dull duration half maximum (FDHM), full width half maximum (FWHM), time to 50% peak amplitude (TF_{50}), Fourier Ring Correlation (FRC), T-tubule (TT), heart failure (HF), ischemic heart disease (IHD).

1. Introduction.

Cardiomyocyte contraction following action potential-(AP)-mediated depolarisation occurs via Excitation Contraction Coupling (ECC) [1, 2]. Activation of Ca^{2+} release from the (SR) via RyRs by Ca^{2+} entering the cell through L-type voltage gated Ca^{2+} channels (LTCC) on the sarcolemma is central to this process. Synchronised activation of RyRs distributed throughout the CM volume in turn generates an homogenous cell-wide increase in intracellular Ca^{2+} and the efficient contraction necessary for pump function [3-5]. This coordinated activation of RyRs throughout the CM is facilitated by T-tubular (TT) invaginations of the sarcolemma that place LTCC at locations opposing SR RyR clusters within 15 nm of each other, forming dyads or couplons [3, 6-8].

In rodents, TT are regularly spaced along the Z-lines of the sarcomeres, whereas, in disease, and in larger mammals, including pigs and in human, TT density is substantially lower [3, 5, 8-12]. With lower TT density, a greater proportion of RyR clusters are not associated with LTCCs (non-coupled, extra dyadic) and therefore not directly activated by Ca^{2+} influx during the AP but by Ca^{2+} diffusing from coupled dyadic RyRs [13, 14]. Consequently, Ca^{2+} release synchrony across the cell during the CaT is reduced, resulting in lower ECC gain, global Ca^{2+} transient amplitude and contractile force [4]. Further, non-coupled RyRs display increased spontaneous Ca^{2+} release in HF, contributing to the initiation of Ca^{2+} waves, which via the electrogenic Na^{+}/Ca^{2+} exchanger (NCX) and altered repolarising K^{+} currents, promote delayed after depolarisations (DADs) and APs that underlie potentially organ-wide arrhythmia [15-20].

Ventricular CMs also express inositol 1,4,5'-trisphosphate receptor ($InsP_3Rs$) Ca^{2+} release channels (the type 2 isoform, $InsP_3R2$) [21-25]; their expression and conductance are however substantially lower than RyRs [26-28]. While induction of inotropy and arrhythmogenic activity have been reported, effects of $InsP_3$-induced Ca^{2+} release (IICR) in healthy CM, are if detected, generally modest and vary between studies and species [23, 25, 29, 30]. In ventricular CMs from hypertrophic or failing rodent hearts, the influence of IICR on CM physiology is greater [23, 31, 32], with increases in CaT amplitude, diastolic Ca^{2+} and frequency of arrhythmogenic events following exposure to $InsP_3$ or neurohormones that promote $InsP_3$ generation such as Angiotensin II (AngII) and Endothelin (ET-1) reported [23, 29, 33, 34]. Despite increased expression in disease, SR Ca^{2+} release via $InsP_3Rs$ is minor relative to via RyRs during the CaT. To explain how this small change in cytosolic [Ca^{2+}] generated by IICR influences ECC, we and others have proposed a mechanism that involves signal amplification by RyRs [23, 25, 35-37]. IICR is also reported to engage proximal NCX, thereby contributing to altered electrophysiology [31].

Despite extensive rodent studies, the role and mechanism of action of IICR in the pathophysiology of ventricular CM of larger mammals are not well defined. Given the substantial differences in the physiology and cellular architecture, including in the coupling of RyRs with the TT membrane, between rodent and large mammals [4, 38], analysis of the role of IICR in this context is vital. Previous studies suggested a contribution of IICR to the arrhythmogenic action of neurohormonal agonists in human HF [31]. However, these studies did not directly probe $InsP_3R$ activity. Recently, by either direct introduction of $InsP_3$ into the cell or generated following AngII stimulation, we described a contribution of $InsP_3R$ activation to the arrhythmogenic action of GPCR agonists in end stage human HF [39].

Moreover, in HF, $InsP_3$ increased Ca^{2+} leak from the SR that on the background of lower SERCA activity present, led to SR Ca^{2+} content depletion and reduced CaT amplitude. Despite these advances, how IICR contributes to human CM physiology during the early stages of remodelling prior to HF observed during ischemic heart disease (IHD) is not determined. The mechanism by which IICR influences Ca^{2+} dynamics at the molecular level is also not fully understood. Given the high incidence of sudden cardiac death and arrhythmias in IHD patients and in the early period following MI, identifying mechanisms underlying pathology in this context is essential [20, 40]. Here we set out to test the hypothesis that IICR plays a dual role in pathological remodelling of CM, whereby it both rescued desynchronised Ca^{2+} release during ECC but also increased spontaneous Ca^{2+} release events that could in turn contribute to arrhythmia. To these ends, we chose an established preclinical pig model of ischemic heart disease where CM in the area adjacent to the infarct undergo substantial remodelling associated with increased arrhythmic activity [41]. Using Ca^{2+} imaging and patch clamp electrophysiology, we established that Ca^{2+} signalling between $InsP_3Rs$ and RyR is important in regulation of Ca^{2+} release and arrhythmogenic activity in post-MI remodelling. We further showed using DNA-PAINT [42] super resolution microscopy the best evidence of co-clustering of $InsP_3Rs$ and RyRs, which we further showed by mathematical modelling could contribute to the functional interactions between these channels observed in MI. Notably, unlike in human, owing to retained SERCA function, IICR did not lead to increased Ca^{2+} leak and SR Ca^{2+} depletion and thus diminished CaT in pig MI CM. Together, these data provide key insights into the mechanism of action of $InsP_3$ signalling in the remodelled heart of large animals and how this may differ from CM in end-stage heart failure.

2. Results

2.1 $InsP_3$ increases synchronicity of SR Ca^{2+} release during ECC without substantially affecting CaT properties.

We examined the influence of IICR on CaT in voltage clamped CM from Sham and MI pig as per the protocol in Figure 1A. Cardiac remodelling after MI determined by MRI is presented in Table S1 and is as previously described [41]. CaT amplitude and time to 50% decay (Figure 1Ci,Cii) were unaltered between Sham and MI CM and no effect of $InsP_3$ was detected. The synchronisation of Ca^{2+} release following cell depolarisation during the CaT was investigated by analysis of the average time to 50% amplitude of the CaT on a pixel by pixel basis (TF_{50}). TF_{50} was significantly greater in MI than in Sham CM at baseline (Figure 1Ciii, left). Notably, $InsP_3$ application significantly reduced TF_{50} in MI but not in Sham (Figure 1Ciii, right). Together, these data reveal the potential for IICR to modulate local Ca^{2+} release and its synchronicity during the CaT in post-MI CM remodelling.

Fig 1

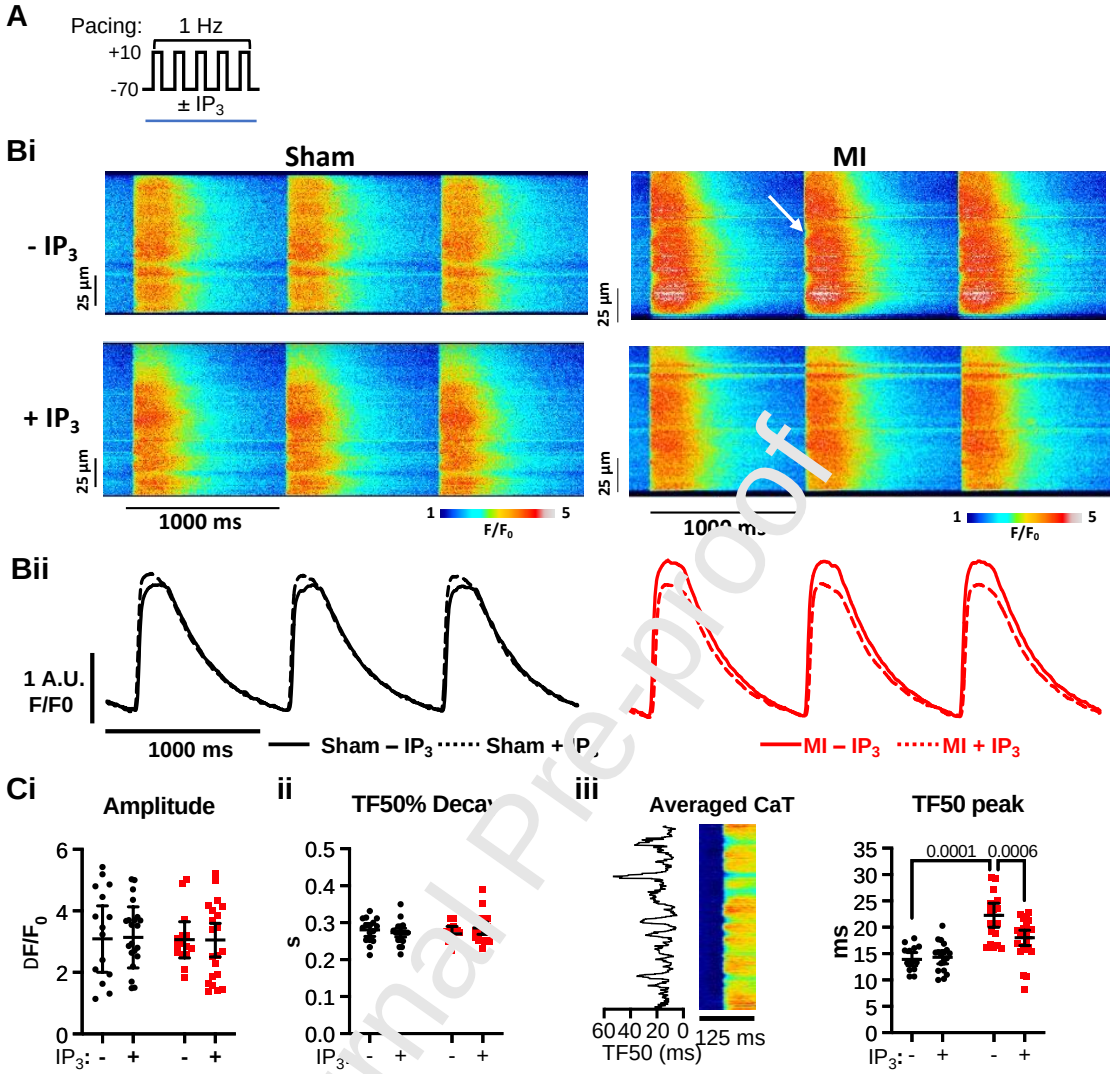

Figure 1. $InsP_3$ accelerates Ca^{2+} release in MI CM. A. Cartoon of experimental protocol. **Bi.** Xt images of CaT recorded by confocal linescan imaging of Fluo-4 in Sham and MI CM in the presence and absence of $InsP_3$ at 1 Hz pacing. **Bii.** Normalised fluorescence traces (F/F0) of CaT described in i. **C.** Summary data of (i) CaT amplitude (ii) time to 50 % decay of the CaT (TF50 decay) and (iii) pixel by pixel averaged time to 50% of CaT peak amplitude (TF_{50}). Left panel: example of averaged Xt image of 5 CaT and time to F_{50} on a pixel by pixel plotted. Right panel: summary data of average TF_{50} calculated as on the left panel. (Sham ±$InsP_3$ n_{cells} =15-18; N_{pigs}=6,6; MI ±$InsP_3$ n_{cells}=15,21; N_{pigs}=5,5). Statistical analysis was by a generalised mixed effect model with Tukey Post hoc analysis.

2.2 $InsP_3$ stimulates increased RyR-dependent sparks in post-MI ventricular CM.

Given that Ca^{2+} sparks are the fundamental units of Ca^{2+} release underlying the CaT, we examined whether they were influenced by IICR. Ca^{2+} sparks were recorded by linescan confocal imaging as in Figure 2A and B. At baseline, Sham and MI CM displayed a low

frequency of Ca^{2+} sparks (Figure 2C). $InsP_3$ significantly increased Ca^{2+} spark frequency in MI CM, whereas it was without effect in Sham (Figure 2B,C). Ca^{2+} spark amplitude, duration (FDHM) and width (FWHM) were unaffected by $InsP_3$ (Figure S2A). The contribution of RyRs to the effect of $InsP_3$ on Ca^{2+} sparks was next determined. RyR inhibition with tetracaine (Tet, 1 mM) significantly reduced Ca^{2+} spark frequency in both Sham and MI CM. Under these conditions of RyR inhibition however, Ca^{2+} release events were observed in more cells at a higher frequency in MI than in Sham (1 from 8 cells in Sham vs 6 from 12 cells in MI, p=0.0425 at frequency 0.0075±0.0075 vs 0.06±0.02 sparks/s/100 µm in sham vs MI; p=0.0441, n=8,12, N=3,3). The contribution of RyR to Ca^{2+} spark properties during $InsP_3$ stimulation was assessed by their analysis before and after Tet treatment as in (Figure S2B). Amplitude of Ca^{2+} release events was significantly reduced in the presence of Tet whereas FWHM and FDHM were unaffected (Figure S2C). Together these data, indicate that increased Ca^{2+} spark activity in MI CM requires both active RyRs and $InsP_3$Rs.

We next determined whether the increased Ca^{2+} spark frequency in MI CM exposed to $InsP_3$ led to greater SR Ca^{2+} leak and SR Ca^{2+} store depletion. In the absence of $InsP_3$, no difference in spark-dependent Ca^{2+} leak from the SR, (spark mass (FWHM.FDHM.Amplitude) x frequency) [43] between Sham and MI CM was observed, whereas with $InsP_3$ it was significantly increased in MI (Figure 2D). Consistent with $InsP_3$Rs enhancing leak via RyRs, the effect of $InsP_3$ was prevented by Tet (Figure 2D). SR Ca^{2+} load was next measured by quantitating the integral of the NCX current during SR store exhaustion with caffeine [44]. In contrast to our findings in human HF, SR load was no different between Sham and MI CM, and no effect of $InsP_3$ on either Sham or MI CM was detected (Figure 2E). SERCA-mediated Ca^{2+} uptake rate was also assessed according to previous methods whereby the rate constant of decay of the electrically-evoked CaT was subtracted from the Caffeine-elicited

Ca^{2+} elevation [45], and found to be no different between Sham and MI (Figure S2D). Together, these data support the notion that in MI CM, $InsP_3$ acts via RyR to increase Ca^{2+} sparks. Moreover, despite increased Ca^{2+} spark-dependent leak, and consistent with no effect of IICR on CaT amplitude, $InsP_3$ did not alter SR Ca^{2+} load.

Fig 2

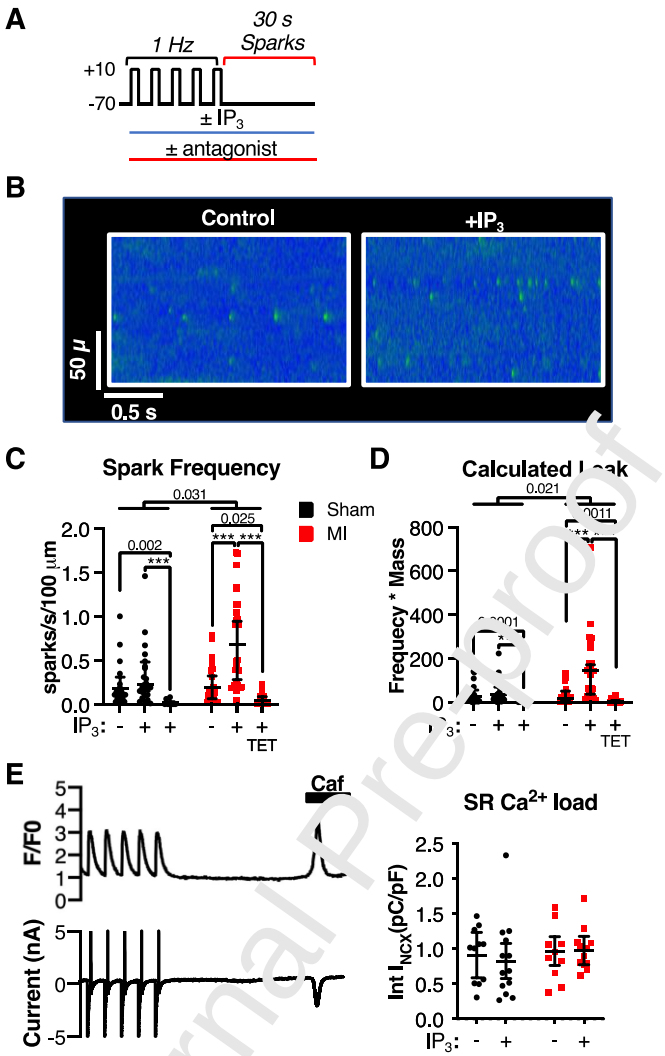

Figure 2. $InsP_3$ increases spark frequency without depleting SR Ca^{2+} stores in MI CM. A. Experimental protocol used for analysis of Ca^{2+} sparks. **B.** Example Xt images of Ca^{2+} sparks acquired by linescan imaging of voltage clamped MI CM in the presence and absence of $InsP_3$. **C.** Summary data of frequency Ca^{2+} spark/events under the conditions shown (for Sham ± $InsP_3$ n_{cells}=19-24; N_{pigs}=6-9; MI ± $InsP_3$ n_{cells}=26-27; N_{pigs}=7-9 ; for Tet in the presence of $InsP_3$, Sham vs MI, n_{cells}=9-12; N_{pigs}=3). **D.** Analysis of total spark mass (FWHM*FDHM*Amplitude*frequency) as a surrogate of spark-dependent leak. **E.** Quantitation of SR Ca^{2+} load by integration of NCX current during Caffeine-mediated Ca^{2+} release. Left panel: example of experimental protocol showing a train of electrically evoked Ca^{2+} transients and the stimulation traces followed by caffeine-mediated Ca^{2+} increase and activation of NCX current (I_{NCX}). Right panel: Summary data of the integrated NCX current in Sham and MI CM in the presence and absence of $InsP_3$ (Sham ± $InsP_3$ n_{cells} =11,13; N_{pigs}=5,6; MI ± $InsP_3$ n_{cells}=10,13; N_{pigs}=4,6). Statistical analysis of C and D was by non-parametric ANOVA with Tukey post hoc analysis and E by a generalised mixed effect model with Tukey Post hoc analysis.

2.3 Alterations in $InsP_3R$ expression and subcellular localisation are observed in MI.

The greater activity of $InsP_3$ in MI CM suggested an increase in expression and/or an alteration in subcellular localisation of $InsP_3Rs$. Increased $InsP_3R$ activity could also be amplified through interaction with RyRs sensitised by CaMKII phosphorylation, which we have previously reported in this model [17]. Immunoblotting revealed a significant increase in $InsP_3R2$ in MI (Figure 3A) while RyR2 expression was unchanged. RyR2 phosphorylated at the serine 2814 CaMKII site (RyR2-pS2814) was however significantly increased (Figure S3A). $InsP_3R2$ mRNA levels (ITPR2) were unaltered as previously described [23], and RyR2 mRNA abundance was decreased (Figure S3B). Immunoblotting showed no significant changes in expression of SERCA2a or NCX (Figure S3C).

The subcellular localisation of $InsP_3R2$ relative to RyRs and of both channels relative to sarcolemmal and TT membranes, labelled with an NCX antibody, was next determined (Figure 3B) [46]. Confocal images were deconvolved and $InsP_3R$ and RyR clusters identified and analysed. RyRs were primarily distributed in a striated pattern along the Z line, where their distribution coincided with the sarcolemma/TT (Figure 3B,C). $InsP_3Rs$ showed a similar distribution as RyRs, although a lower proportion of $InsP_3Rs$ aligned with TT (Figure 3B,C). For both $InsP_3R$ and RyR clusters, no significant difference in their location relative to membrane was detected in MI (Figure 3C). The similarity in the distributions of both channel types was supported by Mander's co-localisation analysis, which showed an overlap of ~ 5% of RyRs with $InsP_3Rs$ and ~ 10% of $InsP_3Rs$ with RyRs (Figure S3D). As cluster area correlates with cluster channel number [47], it was also analysed. RyR cluster area was almost double that of $InsP_3R$ clusters (Figure 3D). No significant change in the area of $InsP_3R$ or RyR clusters

was detected following MI, although for $InsP_3Rs$, this approached significance (Figure 3D).

Fig 3

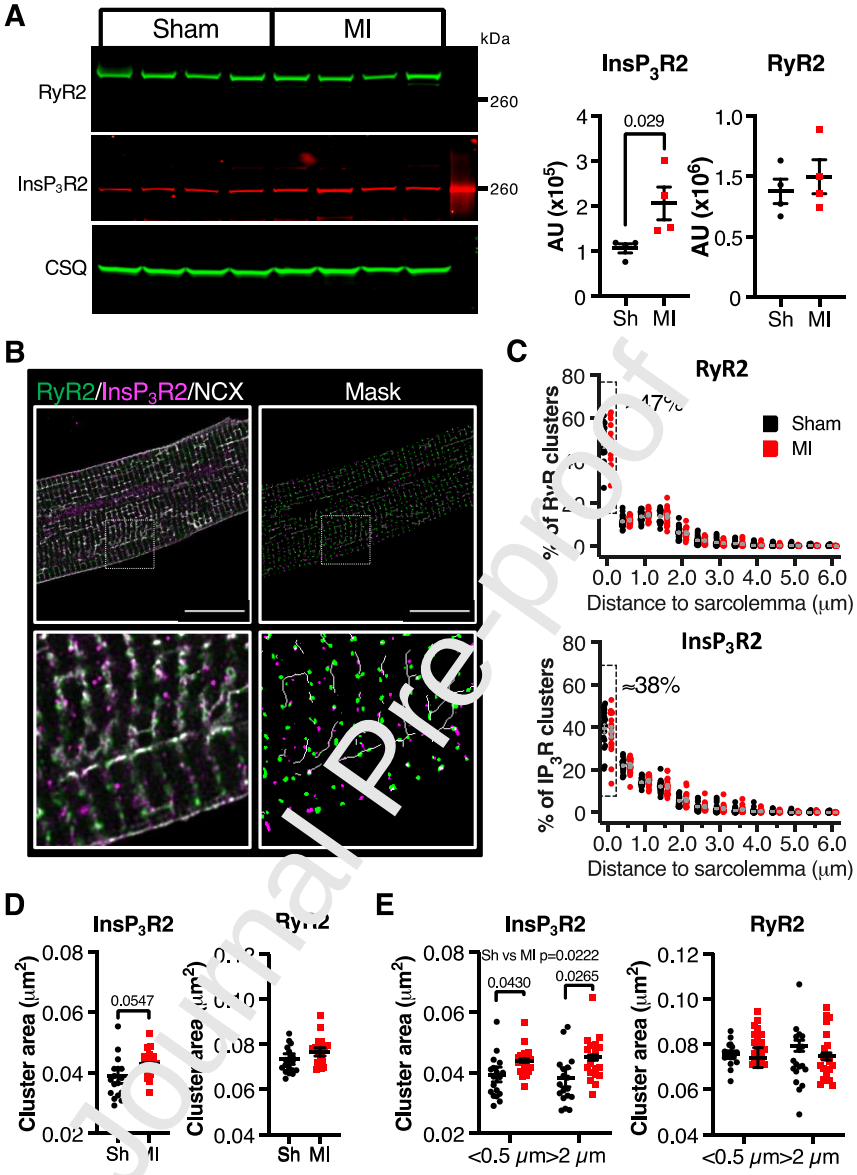

Figure 3. $InsP_3Rs$ are increased in expression in MI and show altered cellular distribution. A. Immunoblot analysis of $InsP_3R$ and RyR in Sham and MI CM (N = 4 and 4 pigs). Left: $InsP_3R2$ (red), RyR2 (green) and CSQ (red) used as a loading control probed on the same blot are shown. Right: Densitometric analysis of $InsP_3R2$ and RyR2 normalised to the abundance of CSQ in the same blot. Analysis by Mann-Whitney test. **B.** Confocal images of an MI CM immunostained with antibodies against $InsP_3R2$ (magenta) and RyR2 (green). TT were stained with antibodies against NCX (white). Scale bar = 20 μ. Images are as follows: top left, deconvolved confocal image; top right, mask of deconvolved image showing distribution of clusters; bottom left, zoom of regions shown in confocal image; bottom right, zoom of masked image. A skeleton of the TT network is also shown in the bottom right image. **C.** Frequency distribution of $InsP_3Rs$ and RyRs relative to a TT membrane in Sham vs MI (Sham n_{cells}=19; N_{pigs}=5; MI n_{cells}=20; N_{pigs}=5). **D.** $InsP_3R2$ and RyR2 cluster areas in Sham and MI. *t*-test. **E.** $InsP_3R2$ and RyR2 cluster areas in Sham and MI plotted according to their location relative to the TT membrane. 2 way ANOVA with Bonferroni post-hoc analysis.

In pig MI CM, we have previously described increased propensity of Ca^{2+} release at sites distal to TT membranes (non-coupled) [48]. We therefore tested whether $InsP_3Rs$ were differentially localised to coupled vs non-coupled RyR clusters. $InsP_3Rs$ and RyRs were categorised according to their distance to the sarcolemma as coupled (<0.5 μ) or non-coupled (>2 μ) [46]. Although, no change in the number of either coupled or non-coupled $InsP_3R$ clusters was observed, clusters area was significantly increased in MI at both regions (Figure 3E). RyR cluster area did not change at either region (Figure 3E). Together, this data suggested the potential for a greater influence of $InsP_3Rs$ on RyRs in MI.

2.4 $InsP_3R$ co-clustering with adjacent RyRs is increased in MI.

To examine whether $InsP_3Rs$ are sufficiently close to RyR to influence their activity, their relative localisation was next determined by DNA-PAINT super resolution microscopy [42]. Fourier Ring Correlation (FRC) of the $InsP_3R$ and RyR labelling data revealed a lateral resolution of ~46 nm [49] (Figure S4A). Consistent with our confocal imaging (Figure 3B), DNA-PAINT showed $InsP_3Rs$ and RyRs to be localised in clusters that were arranged in a striated pattern (Figure 4A). Estimation of the number of receptors accommodated in the stained regions, as described [47, 50], revealed a broad distribution of cluster sizes (Supplementary Figure S4B,C), although many isolated receptors (cluster = 1 in histogram) were also detected. Since clustered channels are considered to underlie Ca^{2+} spark events [51], and that single point data could be contaminated by false-positive localisations, these were excluded from subsequent analysis. Applying these criteria revealed a significant increase in the number of $InsP_3Rs$ per cluster in MI while RyR number per cluster was unchanged (Figure 4B). Using the the proportion of clusters with 2 or more

Fig 4

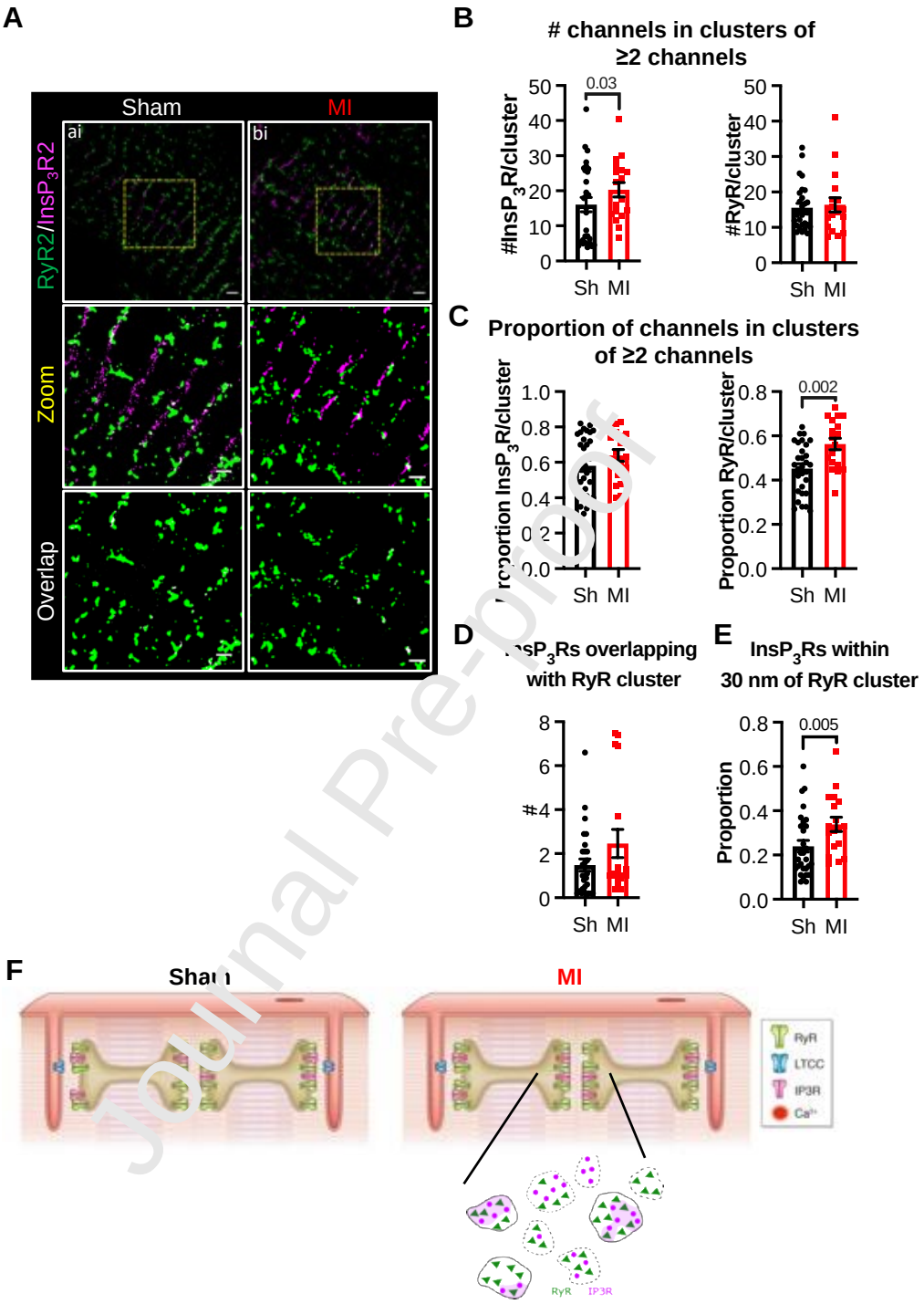

Figure 4. DNA-PAINT analysis of $InsP_3R2$ and RyR2 in Sham and MI. A. DNA-PAINT images of $InsP_3R2$ (magenta) and RyR2 (green) in sections cut from Sham (ai) and MI (bi) cardiac tissue. Scale bar = 1 μ. aii and bii, images show a zoom of the area highlighted in yellow in ai and aii. Aaiii and biii. Distribution of RyRs showing regions of clusters overlapping with $InsP_3R2$ clusters in white. Scale bar = 0.5 μ. **B.** Size of $InsP_3R2$ and RyR2 clusters comprising 2 or more channels represented as number of channels accommodated by labelled area. **C.** Proportion of $InsP_3R2$ or RyR2 clusters in clusters comprising 2 or more channels. **D.** Overlap of $InsP_3Rs$ with RyR clusters of 5 or more channels. **E.** Proportion of $InsP_3Rs$ within 30 nm of edge of RyR cluster**.** Sham $n_{sections}$= 29; N_{pigs}=3; MI $n_{sections}$=18; N_{pigs}=3. Analysis by unpaired *t*-test with Welch correction. **F.** Cartoon summarising data from Figs 3 and 4 showing relative distributions of $InsP_3Rs$ and RyRs at coupled and non-coupled sites and their distribution in clusters.

channels as a measure of cluster size, $InsP_3R$ cluster size was unchanged but RyR cluster size

was significantly increased in MI (Figure 4C). We next investigated whether $InsP_3Rs$ and RyRs co-clustered. Analysis of the overlap of the distributions of the two channel types revealed that on average 2 or more $InsP_3Rs$ overlapped with each RyR cluster, indicating the presence of mixed-channel clusters (Figure 4D). No difference in the number of overlapping $InsP_3Rs$ per RyRs cluster was detected between Sham and MI. To account for $InsP_3Rs$ that could influence RyR activity, we performed a second analysis whereby $InsP_3Rs$ within 30 nm (scale of a single channel) of a RyR cluster were added to the $InsP_3R$ population that overlapped with the RyR clusters. This $InsP_3R$ population was significantly increased in MI (Figure 4E). Together, our analysis identifies for the first time nanoscale co-clustering of $InsP_3Rs$ and RyRs in CM, and moreover, an increase in $InsP_3Rs$ proximal to RyRs in MI (Figure 4F).

2.5 Mathematical modelling predicts influence of non-coupled $InsP_3Rs$ on Ca^{2+} spark generation.

Having shown increased overlap of $InsP_3Rs$ with RyRs clusters, we explored using a mathematical model that incorporates the activity of both RyRs and $InsP_3Rs$ in a Ca^{2+} release site (cluster) [52], whether sensitisation of RyR by Ca^{2+} release via these $InsP_3Rs$ could explain the increase in Ca^{2+} sparks seen in MI CM exposed to $InsP_3$ (Figure 5A and Figure S5A). We particularly examined whether $InsP_3R$-RyR-Ca^{2+} mediated crosstalk within a non-coupled site could facilitate the recruitment of this site by Ca^{2+} diffusing from nearby coupled sites, thereby providing a mechanism for the increased Ca^{2+} sparks in MI at these sites.

To this end, we built on our mathematical model that examined spontaneous spark activity at a dyadic Ca^{2+} release site with a fixed number of RyRs based on published data [51, 53] (orange blocks in Figure S5B) over a varying number of $InsP_3Rs$ (0, 5, 10, or 20 per cluster; magenta blocks in Figure S5B) [52]. We extended this model to examine the effect of $InsP_3Rs$ on Ca^{2+} release at a non-coupled (NC) site under the influence of coupled (C) sites placed equidistant (2 µm centre to centre) on either side (with 10 $InsP_3Rs$), which were either allowed to spontaneously activate (2 C 1 NC C 0 Triggers), or which were triggered, as in ECC, at 1 Hz (2 C 1 NC C 3 Triggers) (Figure 5B,C). Our choice of using a reduced-order representation of the Ca^{2+} release site with 15 RyRs was justified by previous 3D simulations, which showed that the spatial distribution of RyRs in a Ca^{2+} release site was not critical to the Ca^{2+} spark profile when >9 RyRs were in the cluster [54]. Ca^{2+} changes generated by the model are measured in terms of $[Ca^{2+}]$ since they are more informative than simulated fluorescence changes of the Ca^{2+} indicator Fluo-4, which is saturated by the $[Ca^{2+}]$ reaching 10s of µM present in microdomain around the Ca^{2+} release site [55, 56].

200 simulations were performed for each $InsP_3R$ number condition with results obtained from a 2 s period after an initial 1 s wait time for the system to achieve steady state (Figure 5B,C). Consistent with our recent findings [52] and with results presented here (Figure 2C), the chance of observing a spontaneous spark at the non-coupled site in isolation (1 NC 0 Trigger) increased with $InsP_3R$ number (Figure 5C). Ca^{2+} spark amplitude decreased to a minor extent with the number of $InsP_3R$, which we attributed to a depletion of Ca^{2+} at the junctional SR and thus a reduction in the Ca^{2+} gradient between the cytosolic space adjacent to the release site and the SR lumen; whereas Ca^{2+} spark FDHM remained unchanged (Figure S6) [52]. To test whether $InsP_3R$-RyR co-clustering at non-coupled sites led to their

sensitisation and activation by Ca^{2+} diffusing from

Fig 5

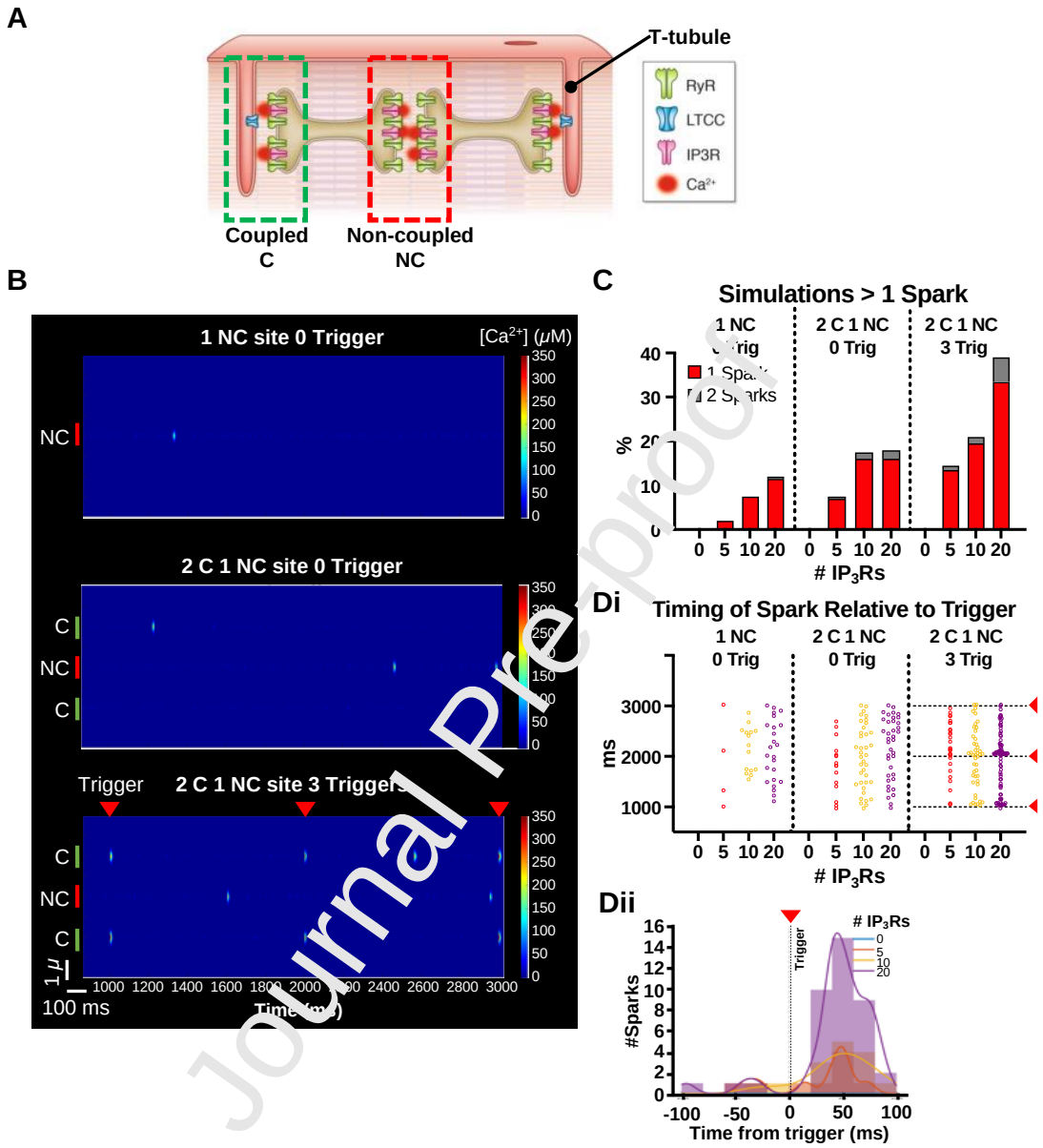

Figure 5. Mathematical modelling supports enhancement of Ca^{2+} sparks at non-coupled sites by $InsP_3$-induced Ca^{2+} release. A. Cartoon showing localization of non-coupled (NC) and coupled (C) Ca^{2+} release sites and how this relates to the setup of the model used for analysis of impact of $InsP_3Rs$ at non coupled sites on Ca^{2+} release at these sites. **B**. Examples of trials performed under the conditions indicated with $[Ca^{2+}]_i$ changes during the Ca^{2+} release events shown. The red arrowheads indicate timings of triggers used to stimulate Ca^{2+} release. The locations of coupled (C) and non-coupled (NC) sites on the simulations is indicated. **C.** Summary data showing percentage of simulations that display Ca^{2+} sparks under the indicated simulation conditions and differing number of $InsP_3Rs$. **D.** Analysis of the timing of Ca^{2+} sparks across the duration of the simulation in simulations presented in A with either 0, 5, 10 or 20 $InsP_3Rs$ present in the non-coupled cluster. **Di.** Swarm plots of Ca^{2+} spark occurrences shown for all simulations. The time points of the triggers used in the 2 C 1 NC with 3 Triggers simulation condition are indicated by dashed lines and red arrow heads. **Dii.** Density function of the Ca^{2+} spark events relative to the Ca^{2+} trigger that is indicated by a dashed line and red arrowhead.

nearby coupled sites, the overall frequency as well as the timing of the Ca^{2+} spark events at the non-coupled site was determined (including relative to the triggered spark in the 2 C 1

NC 3 Triggers condition) (Figure 5B-D). Consistent with this hypothesis, our model showed that spark frequency at the non-coupled site is increased in the presence of neighbouring coupled sites (Figure 5C, Di; 2 C 1 NC 0 Triggers). Importantly, and further showing the role of coupled sites in their activation, Ca^{2+} sparks were most frequent at or soon after triggers were imposed on the coupled sites (Figure 5Di; 2 C 1 NC 3 Triggers). An increased number of simulations with 2 sparks was also detected with increased $InsP_3Rs$ and in the presence of triggers (Figure 5C). The positive effect of triggers on frequency of Ca^{2+} sparks was further validated by fitting a density function to the histogram of the timing of Ca^{2+} sparks that occurred within either 100 ms before or after the first and second trigger (Figure 5Dii). The increase in Ca^{2+} spark occurrence within 100 ms of the triggers was notably absent in the 2 NC 1C 0 Trigger case (Figure 5C), highlighting that the increased occurrence of Ca^{2+} sparks after a trigger was not purely due to simulation stochasticity (Figure 5B-D). This model further predicted that Ca^{2+} release at the non-coupled site is strongly determined by its distance from the coupled site (Figure S6B-E). Indeed, at intersite distances >4 µm, the activity of coupled sites no longer significantly influence that at non-coupled sites. Altogether, these data indicate that while IICR is sufficient to augment Ca^{2+} spark frequency at non-coupled sites in isolation, it also facilitates Ca^{2+} spark generation at non-coupled sites when Ca^{2+} diffuses from activated coupled sites.

2.6 Diminished Ca^{2+} release at non-coupled sites during MI is enhanced by $InsP_3$.

Prompted by this modelling data and the harmonisation of Ca^{2+} release in MI by $InsP_3$ in Figure 1Ciii (decreased average TF_{50} peak across linescan), we tested whether IICR differentially influenced Ca^{2+} release at coupled vs non-coupled sites in Sham and MI.

Release sites were classified as coupled or non-coupled based on their timing of activation during the CaT according to our previously described distance-map algorithm that correlates spatial and temporal Ca^{2+} release profiles [17, 46]. Coupled and non-coupled sites were activated with a TF_{50}<17.7 ms and TF_{50}>27.4 ms of the CaT respectively (Figure 6B). Events with a TF_{50} between these measures were omitted to allow better discrimination between the two regions [46]. The Xt image in Figure 6B shows the identification of Ca^{2+} sparks at coupled and non-coupled sites.

Ca^{2+} sparks were detected at both coupled and non-coupled sites in Sham CM, although their frequency was lower at non-coupled sites (Figure 6Ci,Cii). $InsP_3$ did not affect Ca^{2+} spark frequency at either location in these Sham CM. In MI CM, a low frequency of Ca^{2+} sparks was detected at both coupled and non-coupled sites in the absence of $InsP_3$ but in contrast to Sham, $InsP_3$ significantly increased event frequency, particularly at non-coupled sites (Figure 6Ci,Cii).

Fig 6

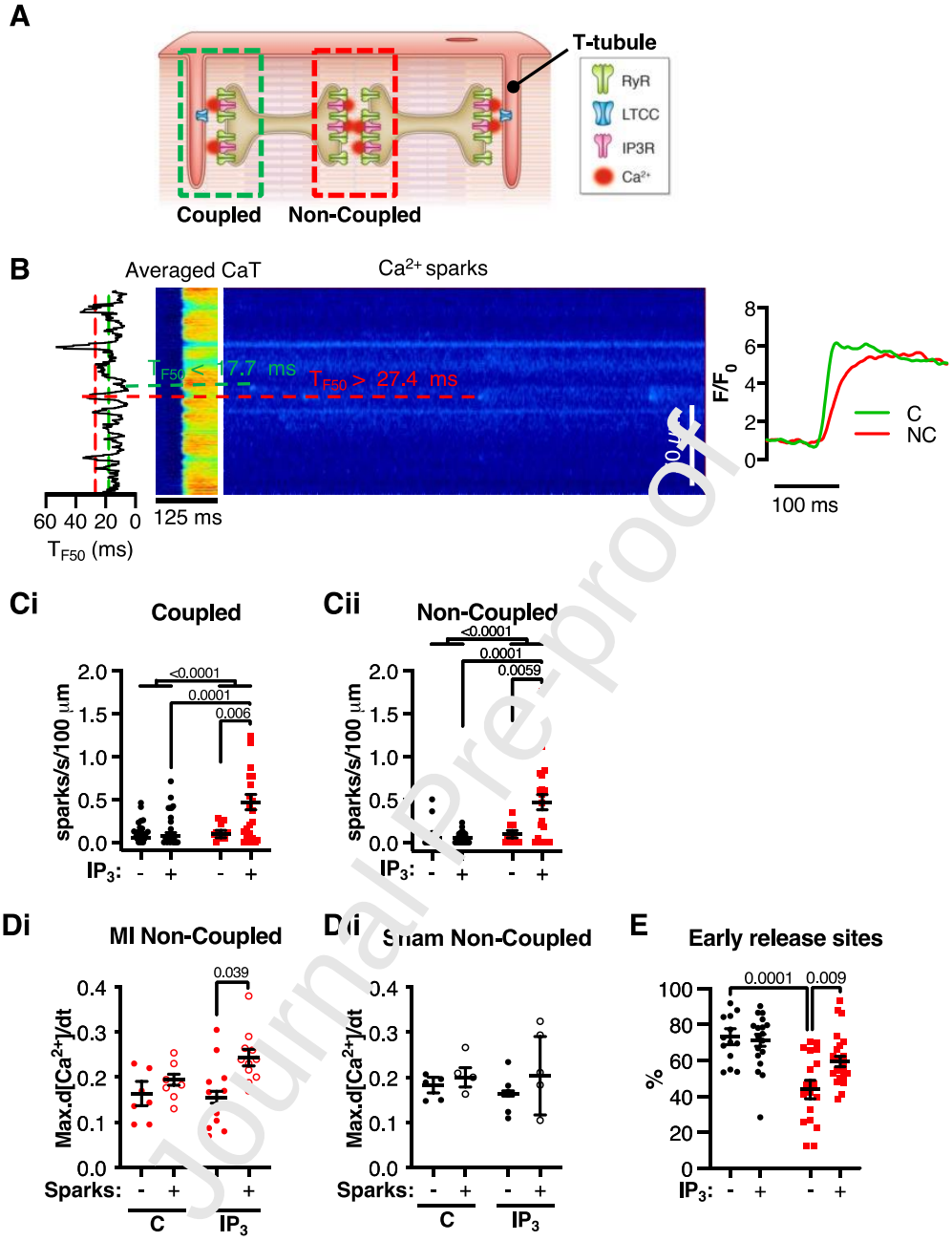

Figure 6. Ca^{2+} release at non-coupled sites is increased by $InsP_3$ in MI. **A.** Cartoon showing location of coupled and non-coupled sites. **B.** Xt image of CaT (middle) with time taken to reach 50% max along the linescan shown (left). An Xt image of the quiescent period subsequent to pacing of the same cell is shown. Ca^{2+} sparks at coupled and non-coupled sites are shown. Coupled sites are classified as those that reach TF_{50} in less than 17.7 ms and non-coupled sites as those that take longer than 27.4 ms to reach TF_{50}. Right: Traces of CaTs in the coupled and non-coupled regions. **C.** Spark frequency at coupled and non-coupled sites in the presence/absence of $InsP_3$ in Sham and MI CM are shown. Ci. Spark frequency at Coupled release sites. Cii. Spark frequency at Non-Coupled release sites. **D.** Comparison of the rate of rise of the CaT at non-coupled sites that either exhibited Ca^{2+} sparks or not when $InsP_3$ was present (i.e. ± activatable $InsP_3Rs$) in MI (Di) vs Sham (Dii) CM. **E.** % of linescan that has a TF_{50} below 17.7 ms (early release sites) in Sham and MI ± $InsP_3$. (Sham ± $InsP_3$: n_{cells}=13,18; N_{pigs}=4,5; MI ± $InsP_3$: n_{cells}=18,23; N_{pigs}=5,5). Statistical analysis was by a generalised mixed effect model with Tukey Post hoc analysis.

Whether IICR augmentation of non-coupled RyR activity acts to accelerate CaT rate of rise uniquely at these sites was next investigated. The rate of rise of the CaT at non-coupled sites that exhibited Ca^{2+} sparks in response to $InsP_3$ (Sparks +; used as a surrogate of

functional $InsP_3Rs$) was determined and compared with non-coupled sites that did not show Ca^{2+} sparks (-) in response to $InsP_3$. Notably, non-coupled sites harbouring functional $InsP_3R$ exhibited enhanced Ca^{2+} release kinetics during CaTs whereas no such increase in CaT kinetics occurred at sites without an increase in Ca^{2+} sparks after exposure to $InsP_3$ (Figure 6Di). $InsP_3$ was without effect on CaT rate of rise at non-coupled or coupled sites in Sham CM or at coupled sites in MI (Supplementary Fig S7), irrespective of the presence of Ca^{2+} sparks.

To determine whether IICR could recruit 'non-coupled' sites and decrease the latency of their activation during the CaT, we analysed whether $InsP_3$ increased the fraction of the linescan that reached TF_{50} at <17.7 ms (coupled sites). At baseline, MI CM exhibited a lower proportion of early Ca^{2+} release sites than Sham (Figure 6E). In the presence of $InsP_3$ however, the % of early response sites was significantly increased, reaching a level similar to Sham. $InsP_3$ did not alter the responsiveness of Ca^{2+} release sites in Sham. These data together point to a special role for $InsP_3Rs$ at non-coupled Ca^{2+} release sites in regulation of CM Ca^{2+} handling in MI. At these locations, $InsP_3Rs$ signal to RyRs enhancing their recruitment and through this mechanism rescue the reduced synchronicity of Ca^{2+} release observed in MI to that in Sham.

2.7 Spontaneous activity is increased by $InsP_3$ in MI.

Ca^{2+} waves arising from non-coupled RyR clusters via NCX lead to arrhythmogenic DADs and APs [17]. Whether IICR engagement of non-coupled RyRs could promote arrhythmogenic activity was therefore determined. To this end, using NCX currents (I_{NCX}) as a reporter of

Ca^{2+} waves, we first examined whether they were increased in MI CM by $InsP_3$. Conditions for increasing wave incidence were generated by pacing at 2 Hz for 1 min and incubation with Isoproterenol (Iso; 10 nM). I_{NCX} events were recorded during 40 s after pacing as per the protocol shown in Figure 7A [17]. In the absence of $InsP_3$, while both Sham and MI CM displayed I_{NCX} events, these events were significantly more frequent in MI (Figure 7B,C). This increased activity was not due to differences between Sham and MI in SR Ca^{2+} uptake rate (Figure S2D). In MI but not in Sham, $InsP_3$ induced an additional significant increase in the frequency of these events (Figure 7B,C). Given the positive relationship between I_{NCX} and APs, the effect of $InsP_3$ on I_{NCX} amplitude in MI CM was also measured. $InsP_3$ significantly increased I_{NCX} amplitude in MI CM exposed to Iso (Figure 7D).

Whether the increase in I_{NCX} events in MI CM translated into increased frequency of DADs and APs was next determined. DADs and APs were recorded as described above albeit, CM were paced and DADs and APs recorded under current clamp during the following 40 s period (Figure 7A)[17]. As no spontaneous activity was observed in the absence of Iso, experiments were only performed in its presence. At baseline, DAD frequency was significantly greater in MI than in Sham CM but no effect of $InsP_3$ was detected for either condition (Figure 7E,F). APs were also rarely detected in Sham or MI CM at baseline (Figure 7E,G). Notably however, AP frequency was uniquely significantly increased by $InsP_3$ in MI CM, with no effect in Sham detected (Figure 7G). This specific action of $InsP_3$ on APs in MI CM was also apparent when the incidence of DAD relative to AP was compared between Sham and MI (Figure 7H). Since greater DAD amplitude increases the propensity for AP generation, whether it was affected by $InsP_3$ was analysed (Figure 7I). While $InsP_3$ had no effect on DAD amplitude in Sham, it significantly increased DAD amplitude in MI, suggesting

that in MI, increasing DAD amplitude contributes to the mechanism by which $InsP_3$ increases APs occurrence.

Fig 7

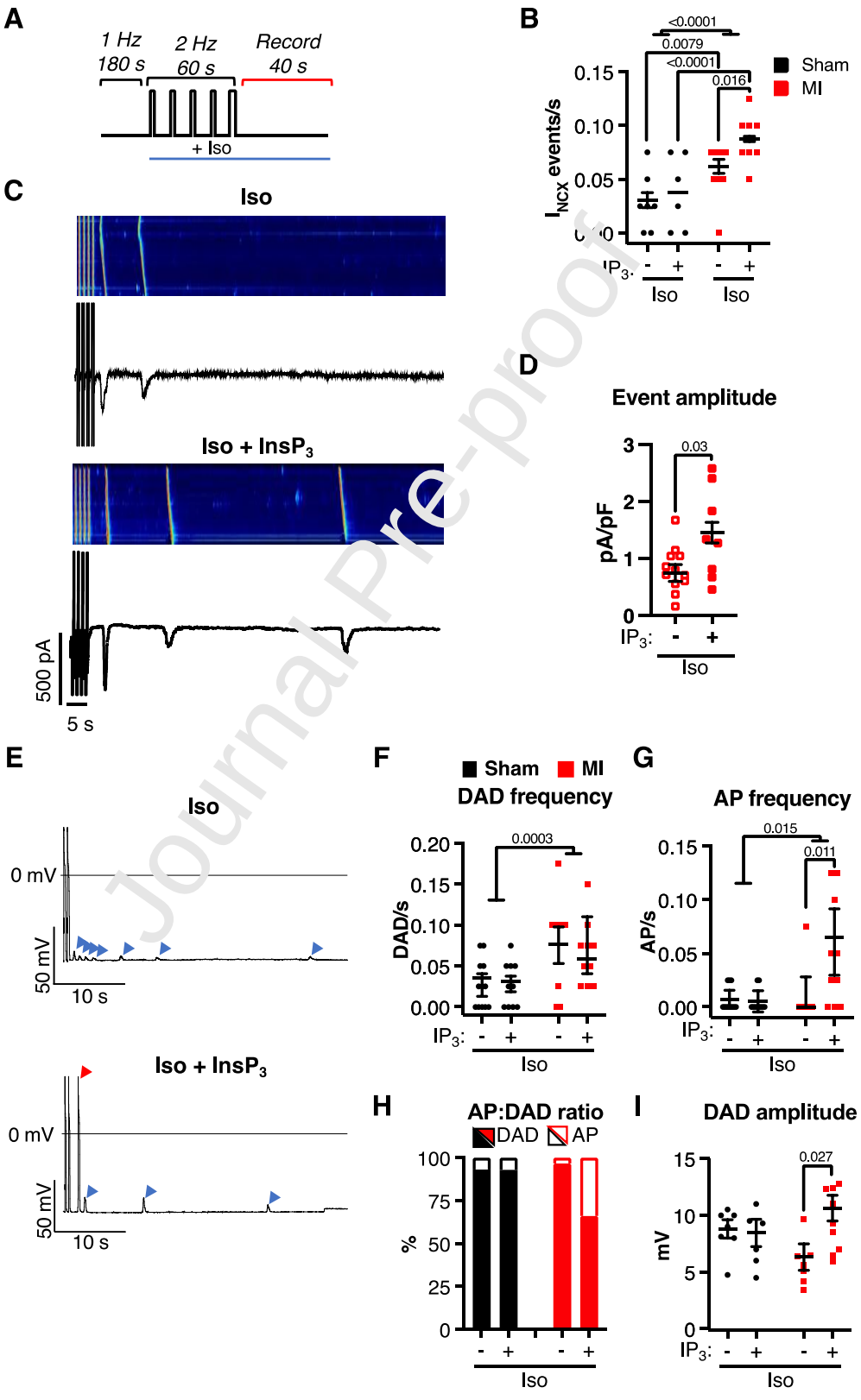

Figure 7. $InsP_3$-induced Ca^{2+} release contributes to increased arrhythmogenic activity in MI CM. A. Cartoon of experimental protocol used for induction of arrhythmogenic Ca^{2+} waves and detection of DADs and APs. For induction of Ca^{2+} waves and the associated I_{NCX} events reported, cells were paced under voltage clamp and NCX activity monitored at resting membrane potential. For detection of DADs and APs, cells were paced in current clamp mode with current injections at 2 Hz for 90 s. CM were perfused with 10 nM Iso. **B.** Summary data showing I_{NCX} events in Sham and MI CM under the conditions shown. (Sham ± $InsP_3$: n_{cells}=7,6; N_{pigs}=3,3; MI ± $InsP_3$: n_{cells}=13,8; N_{pigs}=4,3). **C.** Example Xt plots and associated voltage traces from MI CM in the presence of Iso ± $InsP_3$. 4 stimulation signals (CaT) are shown after which arrhythmogenic activity is observed in the form of Ca^{2+} waves and inward currents. **D.** Amplitude of I_{NCX} events in MI CM exposed to Iso ± $InsP_3$. t-test. **E.** Analysis of DADs and APs. Example current traces from MI CM exposed to Iso ± $InsP_3$. The blue arrow heads indicate DAD activity and the red arrowhead an AP. **F.** Incidence of DADs in Sham and MI CM in the presence and absence of $InsP_3$. **G.** Incidence of APs in Sham and MI CM in the presence and absence of $InsP_3$. **H.** Incidence of APs and DADs as a percentage of total events. **I.** DAD amplitude in Sham and MI ± $InsP_3$. (Sham ± $InsP_3$: n_{cells}=11,10, N_{pigs}=4,4; ± $InsP_3$: n_{cells}=9,10; N_{pigs}=4,4). Statistical analysis was performed in a hierarchical manner with with Tukey post hoc analysis.

Whether alterations in membrane electrophysiology contributed to the increased propensity for DAD and AP generation was also examined. No significant differences in resting membrane potential (RMP) or action potential duration (APD90) were detected between Sham and MI and no effect of $InsP_3$ was observed (Figure S7A,B). An increase in inward NCX current density has also been reported to underlie the effects of $InsP_3$ in mouse CM [31]. While a small effect of $InsP_3$ was detected at extreme negative membrane potentials (-100 and -120 mV) in MI CM, no significant effect of $InsP_3$ at physiological negative membrane potentials was observed in Sham or MI CM (Figure S7C,D). A significant Nickel-sensitive increase in outward current in MI CM following flash photolysis of $InsP_3$ was however detected. The reversal potential of NCX was no different between Sham and MI and was unaffected by $InsP_3$. The increase in outward current elicited by $InsP_3$ in MI CM was lost in cells dialysed with 10 mM BAPTA to chelate intracellular Ca^{2+} demonstrating the Ca^{2+} dependence of the current activated by $InsP_3$ (Figure S7D).

3. Discussion

Unravelling mechanisms underlying altered Ca^{2+} handling during pathological cardiac remodelling is key to development of strategies to mitigate against the associated reduced cardiac function and arrhythmias that lead to sudden cardiac death. Here, in CM from a porcine preclinical model of ischemic heart disease, we show that enhanced Ca^{2+} release via $InsP_3Rs$ contributes to enhanced arrhythmogenic activity and altered Ca^{2+} handling. Specifically, we find that $InsP_3R$ expression is increased in MI and through proximal localisation with and signalling to RyRs at extra dyadic locations, enhance their activity, thereby accelerating Ca^{2+} release during ECC and promoting spontaneous Ca^{2+} release events. These additional Ca^{2+} release events engage NCX, inducing membrane depolarisation and AP generation.

While a number of studies describe a role for $InsP_3$ in regulating ECC in rodents, particularly in disease, the relevance of IICR to pathology in larger mammals, including in human is less investigated, and thus less clear. Although an arrhythmogenic action of $InsP_3Rs$ was proposed in failing human CM over a decade ago, conclusions drawn are undermined by a number of weaknesses [31]. Particularly, conclusions were largely based on extrapolation of effects in mice, $InsP_3R$ function was not directly analysed, and poorly selective $InsP_3R$ antagonists were used to invoke $InsP_3R$ activation as a mechanism underlying arrhythmias provoked by $G\alpha_q$-coupled agonists. Since Xestospongin C, the $InsP_3R$ inhibitor used, is also a potent inhibitor of SERCA [57], its application would increase SR Ca^{2+} leak and depletion, thereby masking the role of $InsP_3Rs$. More recently, we described an arrhythmogenic action of $InsP_3$ in CM and tissue from end-stage HF patients [39]. Unlike in the study of Signore et

al, we directly introduced $InsP_3$ into CM, avoiding potential off target effects of the inhibitors used to modify effects of GPCR agonists. Using 2-APB at a low concentration shown to have limited off target effects [33], we also demonstrated a potent role of $InsP_3$ in the arrhythmogenic action of Ang II in tissue wedges. Since our human study was performed on HF cells and tissue, an understanding of the influence of the GPCR/$InsP_3$R axis during earlier stages of cardiac remodelling during IHD in a large mammal model is still lacking. Insights into arrhythmia mechanisms at these earlier stages of disease, are however, vitally important and clinically relevant since sudden cardiac death in IHD is highly prevalent in early stages after MI before frank HF [20, 40]. In this regard, the pig preclinical model used in this study is highly relevant, sharing features including increased arrhythmia propensity, observed during the substantial remodelling after MI in human but in the absence of associated co-morbidities [17].

GPCR agonists that we and others have previously used to stimulate $InsP_3$ production in CM also engage multiple kinase cascades which in turn influence the activity of NCX, L-type current, myofilaments and NHE with consequences for Ca^{2+} dynamics and contractility [25, 31, 34, 58, 59]. Since we aimed in this study to specifically probe the influence of $InsP_3$R activation on CM physiology, we chose to directly activate $InsP_3$Rs with $InsP_3$. In line with previous observations in healthy rat and mouse, no effects of $InsP_3$ on CaTs were detectable [23, 33, 60, 61]. This contrasts with that in rabbit, where $InsP_3$ causes an increase in CaT amplitude and with our analysis in human HF where CaT amplitude was reduced [29]. The minimal contribution of $InsP_3$ to the CaT in these healthy pig CM is also consistent with the low abundance of $InsP_3$Rs in ventricular CM [17, 23, 27, 35, 60].

In large mammals, such as pig, and as in rodents, TT density and coupling of LTCC and RyRs is decreased in pathology leading to decreased synchronicity of Ca^{2+} release with

deleterious consequences for CaT generation and contraction [10, 17, 62]. In this model of early post-MI remodelling, while we cannot rule out LTCC redistribution, we previously did not detect alteration of I_{CaL} in MI and thus do not consider it a major contributor to reduced synchronicity of Ca^{2+} release in the MI CM described here [17]. Significantly, Ca^{2+} release heterogeneity was reduced by $InsP_3$, to a level approaching that in Sham. In this manner, $G\alpha_q$-coupled agonists, acting via $InsP_3$ could elicit a beneficial effect to rescue disease-associated decline in cardiac function, analogous to that observed for β-agonists, which recruits Ca^{2+} release at non-coupled sites [63]. In contrast to the mechanism for β stimulation however, which involves increasing store load, enhancing I_{CaL} and sensitising RyR Ca^{2+} release channels via phosphorylation [1], store loading was unaffected by $InsP_3$, suggesting that RyRs are recruited through an alternative mechanism involving increased $[Ca^{2+}]$ in their local vicinity arising from neighbouring $InsP_3Rs$.

Analysis of Ca^{2+} sparks provided deeper insights into the remodelling and mechanism of action of IICR in MI CM, particularly how IICR could recruit non-coupled RyR clusters. Although no difference in Ca^{2+} spark activity was detected between Sham and MI at baseline, in response to $InsP_3$, MI CM exhibited significantly increased Ca^{2+} spark frequency, which was also apparent as a greater Ca^{2+} spark-dependent leak. The similar Ca^{2+} spark frequencies in MI and Sham CM at baseline, which reflect our previous findings at low pacing frequency [17], would indicate that increased $InsP_3R$ expression in MI CM does not in itself lead to greater basal Ca^{2+} release. Further, SR load was no different between Sham and MI and was not affected by $InsP_3$, indicating, that in MI CM, IICR did not act to deplete SR Ca^{2+} stores. These results contrast with our findings in human HF and those from a mouse CM transgenically overexpressing $InsP_3R2$, which show elevated baseline spark activity [39, 64]. In human HF, we found that Ca^{2+} spark frequency and and spark-dependent leak were

increased in the presence of $InsP_3$ leading to a depletion of the SR Ca^{2+} store and reduced CaT amplitude [39]. A key difference however between CM from MI pig and HF human is the substantially reduced activity and expression of SERCA-mediated Ca^{2+} clearance from the cytosol in human, which we show here is unchanged beteen Sham and MI pig CM. In the face of this reduced SERCA activity, the increased leak induced by $InsP_3$ is not re-sequestered ino the store but leads to SR Ca^{2+} depletion. In mouse, increased Ca^{2+} leak in the $InsP_3R2$ transgenic background was proposed to protect the SR from Ca^{2+} overload and Ca^{2+} wave initiation. This was not seen in human HF however, where Ca^{2+} waves were increased by $InsP_3$ [39]. Apart from substantial $InsP_3R2$ overexpression (12 fold), $InsP_3R2$ transgenic mice only show mild hypertrophy and do not exhibit other aspects of a HF CM that would contribute to arrhythmogenic activity such as altered repolarisation currents [64]. As we determined in human but not here in pig, the $InsP_3R$ transgenic mice also exhibit a substantial reduction in RyR expression, which would alter the relative contributions of these Ca^{2+} channels to Ca^{2+} handling.

In agreement with previous findings in rat and human proposing a role for RyRs in amplifying Ca^{2+} release via $InsP_3Rs$ [23, 35, 39, 65], active RyRs were required for $InsP_3$ to increase Ca^{2+} spark frequency and spark dependent leak in MI CM. The premise of this hypothesis is that Ca^{2+} release from $InsP_3Rs$ in the vicinity of co-localised RyRs leads to their sensitisation. Modelling data suggests that [Ca^{2+}] in the 10s of μM would be required at the location of RyRs for this mechanism to be effective [56]. Given that Ca^{2+} steeply declines with distance from its peak in the 100s of μM at a Ca^{2+} channel mouth (e.g. RyR), for any neighbouring channel to influencing a RyR, it would need to be highly proximally localised [51, 56]. While this is established for RyRs in a cluster, single molecule data that places $InsP_3Rs$ sufficiently close to RyRs is lacking. Here and elsewhere, we and others have shown

by confocal imaging localization of $InsP_3Rs$ to the Z-line, where they colocalize to a certain extent with RyRs [23, 66, 67]. While in our recent analysis in human HF, we used STED microscopy to examine $InsP_3R$-RyR relative distributions [39], the resolution of this modality of microscopy may not be sufficient to resolve between clusters of different scales and to establish channel proximities. To overcome these issues, we employed DNA-PAINT super resolution imaging, which can achieve sub 10 nm resolution [42]. We definitively identified $InsP_3Rs$ residing in amongst RyRs in a cluster, thereby enabling Ca^{2+}-mediated channel crosstalk. The number of RyRs per cluster described here was similar to that previously described using super resolution approaches [14, 42, 47, 68]. However, although as previously reported in HF [14], the number of RyR channels per cluster were not increased in post-MI pig CM, we found an increased proportion of larger RyR clusters in MI. Cluster size has important consequences for spark generation in that larger clusters show greater fidelity in spark generation and thus make a greater contribution to spark frequency [53, 69]. In disease however, decreased organization and/or density of RyRs within the cluster leads to a reduced Ca^{2+} dependent coupling between RyRs and reduced kinetics of Ca^{2+} release [14, 70]. The increased proportion of RyR clusters comprising 2 or more channels together with the lack of change in RyR expression (established by immunoblot) in MI that we found are consistent with greater numbers of RyR in the clusters described. The identification of $InsP_3Rs$ residing amongst RyRs in these clusters may represent a mechanism to rescue intra as well as inter cluster coupling, irrespective of whether the neighbouring clusters contain $InsP_3Rs$. Indeed, our modelling data shows that by providing extra Ca^{2+}, by means of an increased number of $InsP_3Rs$, particularly in the immediate vicinity of RyRs, the coupling of stochastically opening RyRs in a cluster is increased, resulting in increased likelihood of a Ca^{2+} spark. Our modelling data also suggest that the presence of $InsP_3Rs$

within a RyR cluster serves to sensitise the cluster to Ca^{2+} diffusing from neighbouring coupled clusters during their activation by an electrical trigger. Consistent with these findings, our cellular analysis showed synchronization of Ca^{2+} release during the CaT by $InsP_3$ in MI. Further supporting this hypothesis, $InsP_3$ preferentially augmented Ca^{2+} sparks and Ca^{2+} release kinetics form non-coupled sites in MI. Moreover, $InsP_3R$ were enriched at non-coupled sites in MI CM. In this way, enhanced IICR could act in positive as well as a deleterious role in disease. These conclusions regarding $InsP_3R$-RyR crosstalk agree with that previously hypothesised but were not substantiated due to the absence of super resolution imaging of $InsP_3R$ distributions and the modelling approaches that we now report in this study [23, 35]. This preferential regulation of Ca^{2+} release at non-coupled sites is reminiscent of that which we previously described in MI pig CM, where increased Ca^{2+} sparks at non-coupled sites were dependent upon CaMKII activity and reactive oxygen species [17]. Indeed, consistent with the known phosphorylation of RyRs in cardiac pathology, we here observed increased levels of CaMKII phosphorylated RyRs in cardiac tissue from MI pigs. While our modelling data suggest that CaMKII is not required for Ca^{2+} release via $InsP_3Rs$ to influence neighbouring RyR, CaMKII phosphorylated RyRs at non-coupled sites likely create a sensitised substrate upon which Ca^{2+} release via $InsP_3Rs$ can preferentially act to augment RyR-mediated Ca^{2+} release at these sites. CaMKII can also phosphorylate $InsP_3R2$ [71], although since this phosphorylation event suppresses $InsP_3R$ activity, it is unlikely to contribute to the increased $InsP_3R$ activity observed in MI CM, which we describe in this manuscript. Given the importance of CaMKII phosphorylation of RyRs in cardiac pathology, contributing to enhanced Ca^{2+} leak and induction of arrhythmias [72, 73], future studies to assess the interaction between IICR, CaMKII, RyRs and Ca^{2+} release will be important to perform.

Arrhythmogenic electrophysiological activity was significantly increased by $InsP_3$ in MI CM. This effect was not due to a substantial increase in inward NCX current as previously reported or that is induced by GPCR agonists [31, 74]. Rather, and in line with findings in human HF [39], our data indicate that dysregulation of intracellular Ca^{2+} handling, including increased spontaneous Ca^{2+} release events via $InsP_3R$-RyR coupling, contribute through activation of NCX to the generation of arrhythmogenic DADs and APs [19]. Previously, we have shown that Ca^{2+} waves underlying arrhythmogenic activity in MI arise from Ca^{2+} release at hyperactive non-coupled RyR clusters [17]. The increased Ca^{2+} sparks at non-coupled sites together with the greater arrhythmogenic activity in MI CM in the presence of $InsP_3$ would suggest a similar model. Notably, and underlining the importance of IICR in disease, $InsP_3$ promoted the almost exclusive generation of APs in MI CM, whereas in Sham, DADs were more prevalent. Supporting increased activation of NCX as a mechanism by which $InsP_3$ crosstalk with RyRs enhance APs, DAD amplitude was greater in MI in the presence of $InsP_3$. The greater potential for $InsP_3$ to promote APs in MI also likely involves an alteration in repolarisation currents such as in I_{K1}, which we have previously reported in this model,[20]. Together, these data re-enforce the notion that mechanisms involving dysregulated Ca^{2+} release leading to membrane depolarisation via NCX are important contributors to the potentially fatal arrhythmic activity associated with remodelling after MI [19].

Conclusions. Here, we have demonstrated increased activity of the $InsP_3/InsP_3R/Ca^{2+}$ signalling pathway in ventricular CM from pig during remodelling after MI. This analysis in pig CM from early stages of IHD is an important step in understanding the role of

GPCR/$InsP_3$-signalling in disease evolution and occurrence of arrhythmias in the progression to HF in human. Our analysis also sheds light on the involvement of $G\alpha_q$ coupled GPCRs including AngII, ET-1 and catecholamines in cardiac pathophysiology. Not only are these mediators found to be elevated in cardiac disease, inhibitors of their activity, for example of the renin angiotensin system, decrease the incidence of arrhythmias in animal models [75] and in patients with IHD [76]. Our findings therefore identify an important and disease-related signalling pathway that may be targeted pharmacologically to prevent fatal arrhythmias.

Author Contributions

Conceptualisation Ideas; X.J, K.S, H.L.R. Data curation and Formal analysis; X.J., A.M., A.T., K.D., E.D., R.D.P., M.A., P.C., C.C., V.R., K.S., H.L.R. Investigation; X.J., A.M., A.T., K.D., E.D., R.D.P., M.A., P.C., C.C., V.R., K.S., H.L.R. Writing - Original Draft Preparation; X.J., H.L.R. Writing - Review & Editing; all authors. Resource provision; K.S., P.C., C.S., V.R., H.L.R. Supervision Oversight and Leadership; K.S., P.C., C.S., V.R., H.L.R.

Declaration of Competing interests

The authors declare no conflicts of interest.

Acknowledgements

This work was supported by the Fund for Scientific Research-Flanders (FWO projects G.0617.09 and G.0918.15 to KRS, FWO Project grant G08861N and FWO Odysseus Project 90663 to HLR; FWO postdoctoral fellowships to ED and GG; FWO PhD fellowship to MA). CS'

contributions were supported by the Human Frontier Science Program (No. 0027/2013), the Engineering and Physical Sciences Research Council of the UK (No. EP/N008235/1) and Biotechnology and Biological Sciences Research Council Grants BB/P026508/1 and BB/T007176/1. This research was supported in part by the Australian Government through the Australian Research Council Discovery Projects funding scheme (project DP170101358) to VR. We thank Patricia Holemans and Roxane Menten for technical assistance and Dr Alexander Clowsley for assistance in preparation and staining of cardiac tissue for DNA-PAINT analysis.

References:

[1] D.M. Bers, Cardiac excitation-contraction coupling, Nature 415(6868) (2002) 198-205.
[2] G. Gilbert, K. Demydenko, E. Dries, R.D. Puertas, X. Jin, K. Sipido, H.L. Roderick, Calcium Signaling in Cardiomyocyte Function, Cold Spring Harb Perspect Biol 12(3) (2020).
[3] A.M. Gomez, H.H. Valdivia, H. Cheng, M.R. Lederer, L.F. Santana, M.B. Cannell, S.A. McCune, R.A. Altschuld, W.J. Lederer, Defective excitation-contraction coupling in experimental cardiac hypertrophy and heart failure, Science 276(5313) (1997) 800-6.
[4] F.R. Heinzel, N. Macquaide, L. Biesmans, K. Sipido, Dyssynchrony of Ca2+ release from the sarcoplasmic reticulum as subcellular mechanism of cardiac contractile dysfunction., J Mol Cell Cardiol 50(3) (2011) 390-400.
[5] L.S. Song, E.A. Sobie, S. McCulle, W.J. Lederer, C.W. Balke, H. Cheng, Orphaned ryanodine receptors in the failing heart, Proc Natl Acad Sci U S A 103(11) (2006) 4305-10.
[6] C. Franzini-Armstrong, Functional implications of RyR-dHPR relationships in skeletal and cardiac muscles, Biol Res 37(4) (2004) 507-12.
[7] C. Franzini-Armstrong, F. Protasi, P. Tijskens, The assembly of calcium release units in cardiac muscle, Ann N Y Acad Sci 1047 (2005) 76-85.
[8] F.R. Heinzel, V. Bito, P.G. Volders, G. Antoons, K. Mubagwa, K.R. Sipido, Spatial and temporal inhomogeneities during Ca2+ release from the sarcoplasmic reticulum in pig ventricular myocytes, Circ Res 91(11) (2002) 1023-30.
[9] I. Jayasinghe, D. Crossman, C. Soeller, M. Cannell, Comparison of the organization of T-tubules, sarcoplasmic reticulum and ryanodine receptors in rat and human ventricular myocardium, Clin Exp Pharmacol Physiol 39(5) (2012) 469-76.
[10] A. Guo, C. Zhang, S. Wei, B. Chen, L.S. Song, Emerging mechanisms of T-tubule remodelling in heart failure, Cardiovasc Res 98(2) (2013) 204-15.
[11] F.R. Heinzel, V. Bito, L. Biesmans, M. Wu, E. Detre, F. von Wegner, P. Claus, S. Dymarkowski, F. Maes, J. Bogaert, F. Rademakers, J. D'Hooge, K. Sipido, Remodeling of T-tubules and reduced synchrony of Ca2+ release in myocytes from chronically ischemic myocardium, Circ Res 102(3) (2008) 338-46.

[12] C.H. Orchard, M. Pasek, F. Brette, The role of mammalian cardiac t-tubules in excitation-contraction coupling: experimental and computational approaches, Exp Physiol 94(5) (2009) 509-19.
[13] P. Asghari, D.R. Scriven, M. Ng, P. Panwar, K.C. Chou, F. van Petegem, E.D. Moore, Cardiac ryanodine receptor distribution is dynamic and changed by auxiliary proteins and post-translational modification, Elife 9 (2020).
[14] T.R. Kolstad, J. van den Brink, N. MacQuaide, P.K. Lunde, M. Frisk, J.M. Aronsen, E.S. Norden, A. Cataliotti, I. Sjaastad, O.M. Sejersted, A.G. Edwards, G.T. Lines, W.E. Louch, Ryanodine receptor dispersion disrupts Ca(2+) release in failing cardiac myocytes, Elife 7 (2018).
[15] H. Dridi, A. Kushnir, R. Zalk, Q. Yuan, Z. Melville, A.R. Marks, Intracellular calcium leak in heart failure and atrial fibrillation: a unifying mechanism and therapeutic target, Nat Rev Cardiol (2020).
[16] A.P. Landstrom, D. Dobrev, X.H.T. Wehrens, Calcium Signaling and Cardiac Arrhythmias, Circ Res 120(12) (2017) 1969-1993.
[17] E. Dries, D.J. Santiago, G. Gilbert, I. Lenaerts, B. Vandenberk, C.K. Nagaraju, D.M. Johnson, P. Holemans, H.L. Roderick, N. Macquaide, P. Claus, K.R. Sipido, Hyperactive ryanodine receptors in human heart failure and ischaemic cardiomyopathy reside outside of couplons, Cardiovasc Res 114(11) (2018) 1512-1524.
[18] K. Schlotthauer, D.M. Bers, Sarcoplasmic reticulum Ca(2+) release causes myocyte depolarization. Underlying mechanism and threshold for triggered action potentials, Circ Res 87(9) (2000) 774-80.
[19] S.M. Pogwizd, D.M. Bers, Cellular basis of triggered arrhythmias in heart failure, Trends Cardiovasc Med 14(2) (2004) 61-6.
[20] M. Amoni, E. Dries, S. Ingelaere, D. Vermoortele, H.L. Roderick, P. Claus, R. Willems, K.R. Sipido, Ventricular Arrhythmias in Ischemic Cardiomyopathy-New Avenues for Mechanism-Guided Treatment, Cells 10(10) (2021).
[21] A.V. Zima, L.A. Blatter, Inositol-1,4,5-trisphosphate-dependent Ca(2+) signalling in cat atrial excitation-contraction coupling and arrhythmias, J Physiol 555(Pt 3) (2004) 607-15.
[22] X. Wu, T. Zhang, J. Bossuyt, X. Li, T.A. McKinsey, J.R. Dedman, E.N. Olson, J. Chen, J.H. Brown, D.M. Bers, Local InsP3-dependent perinuclear Ca2+ signaling in cardiac myocyte excitation-transcription coupling, J Clin Invest 116(3) (2006) 675-82.
[23] D. Harzheim, M. Movassagh, R.S. Foo, O. Ritter, A. Tashfeen, S.J. Conway, M.D. Bootman, H.L. Roderick, Increased InsP3Rs in the junctional sarcoplasmic reticulum augment Ca2+ transients and arrhythmias associated with cardiac hypertrophy, Proc Natl Acad Sci U S A 106(27) (2009) 11406-11.
[24] S. Ljubojevic, S. Radulovic, G. Leitinger, S. Sedej, M. Sacherer, M. Holzer, C. Winkler, E. Pritz, T. Mittler, A. Schmidt, M. Sereinigg, P. Wakula, S. Zissimopoulos, E. Bisping, H. Post, G. Marsche, J. Bossuyt, D.M. Bers, J. Kockskamper, B. Pieske, Early remodeling of perinuclear Ca2+ stores and nucleoplasmic Ca2+ signaling during the development of hypertrophy and heart failure, Circulation 130(3) (2014) 244-55.
[25] K. Demydenko, S. Ekhteraei-Tousi, H.L. Roderick, Inositol 1,4,5-trisphosphate receptors in cardiomyocyte physiology and disease, Philos Trans R Soc Lond B Biol Sci 377(1864) (2022) 20210319.
[26] J.K. Foskett, C. White, K.H. Cheung, D.O. Mak, Inositol trisphosphate receptor Ca2+ release channels, Physiol Rev 87(2) (2007) 593-658.
[27] P. Lipp, M. Laine, S.C. Tovey, K.M. Burrell, M.J. Berridge, W. Li, M.D. Bootman, Functional InsP3 receptors that may modulate excitation-contraction coupling in the heart, Curr Biol 10(15) (2000) 939-42.
[28] P.J. Perez, J. Ramos-Franco, M. Fill, G.A. Mignery, Identification and functional reconstitution of the type 2 inositol 1,4,5-trisphosphate receptor from ventricular cardiac myocytes, J Biol Chem 272(38) (1997) 23961-9.
[29] T.L. Domeier, A.V. Zima, J.T. Maxwell, S. Huke, G.A. Mignery, L.A. Blatter, IP3 receptor-dependent Ca2+ release modulates excitation-contraction coupling in rabbit ventricular myocytes, Am J Physiol Heart Circ Physiol 294(2) (2008) H596-604.

[30] T. Horn, N.D. Ullrich, M. Egger, 'Eventless' InsP3-dependent SR-Ca2+ release affecting atrial Ca2+ sparks., J Physiol 591(Pt 8) (2013) 2103-2111.
[31] S. Signore, A. Sorrentino, J. Ferreira-Martins, R. Kannappan, M. Shafaie, F. Del Ben, K. Isobe, C. Arranto, E. Wybieralska, A. Webster, F. Sanada, B. Ogorek, H. Zheng, X. Liu, F. Del Monte, D.A. D'Alessandro, O. Wunimenghe, R.E. Michler, T. Hosoda, P. Goichberg, A. Leri, J. Kajstura, P. Anversa, M. Rota, Inositol 1, 4, 5-trisphosphate receptors and human left ventricular myocytes, Circulation 128(12) (2013) 1286-97.
[32] M.I. Garcia, D. Boehning, Cardiac inositol 1,4,5-trisphosphate receptors, Biochim Biophys Acta Mol Cell Res 1864(6) (2017) 907-914.
[33] A. Proven, H.L. Roderick, S.J. Conway, M.J. Berridge, J.K. Horton, S.J. Capper, M.D. Bootman, Inositol 1,4,5-trisphosphate supports the arrhythmogenic action of endothelin-1 on ventricular cardiac myocytes, J Cell Sci 119(Pt 16) (2006) 3363-75.
[34] F.M. Drawnel, C.R. Archer, H.L. Roderick, The role of the paracrine/autocrine mediator endothelin-1 in regulation of cardiac contractility and growth., Br J Pharmacol 168(1) (2013) 296-317.
[35] M. Wullschleger, J. Blanch, M. Egger, Functional local crosstalk of inositol 1,4,5-trisphosphate receptor- and ryanodine receptor-dependent Ca2+ release in atrial cardiomyocytes, Cardiovasc Res 113(5) (2017) 542-552.
[36] A.V. Zima, E. Bovo, D.M. Bers, L.A. Blatter, Ca2+ spark-dependent and -independent sarcoplasmic reticulum Ca2+ leak in normal and failing rabbit ventricular myocytes, J Physiol 588(23) (2010) 4743-4757.
[37] K. Demydenko, K.R. Sipido, H.L. Roderick, Ca2+ release via InsP3Rs enhances RyR recruitment during Ca2+ transients by increasing dyadic [Ca2+] in cardiomyocytes, J Cell Sci 134(14) (2021).
[38] I. Smyrnias, W. Mair, D. Harzheim, S.A. Walker, H.L. Roderick, M.D. Bootman, Comparison of the T-tubule system in adult rat ventricular and atrial myocytes, and its role in excitation-contraction coupling and inotropic stimulation, Cell Calcium 47(3) (2010) 210-23.
[39] X. Jin, M. Amoni, G. Gilbert, E. Dries, R. Doñate Puertas, A. Tomar, C.K. Nagaraju, A. Pradhan, D.I. Yule, T. Martens, R. Menten, P. Vanden Berghe, F. Rega, K. Sipido, H.L. Roderick, InsP3R–RyR Ca2+ channel crosstalk facilitates arrhythmias in the failing human ventricle, Basic Research in Cardiology 117(1) (2022) 60.
[40] S. Allender, P. Scarborough, V. Peto, M. Raynor, J. Leal, R. Luengo-Fernandez, A. Gray, European cardiovascular disease statistics 2008 Edition, (2007) 1 - 112.
[41] E. Dries, M. Amoni, B. Vandenberk, D.M. Johnson, G. Gilbert, C.K. Nagaraju, R.D. Puertas, M. Abdesselem, D.J. Santiago, H.L. Roderick, P. Claus, R. Willems, K.R. Sipido, Altered adrenergic response in myocytes bordering a chronic myocardial infarction underlies in vivo triggered activity and repolarization instability, J Physiol (2020).
[42] I. Jayasinghe, A.H. Clowsley, R. Lin, T. Lutz, C. Harrison, E. Green, D. Baddeley, L. Di Michele, C. Soeller, True Molecular Scale Visualization of Variable Clustering Properties of Ryanodine Receptors, Cell Rep 22(2) (2018) 557-567.
[43] F.A. Hilliard, D.S. Steele, D. Laver, Z. Yang, S.J. Le Marchand, N. Chopra, D.W. Piston, S. Huke, B.C. Knollmann, Flecainide inhibits arrhythmogenic Ca2+ waves by open state block of ryanodine receptor Ca2+ release channels and reduction of Ca2+ spark mass, J Mol Cell Cardiol 48(2) (2010) 293-301.
[44] A. Varro, N. Negretti, S.B. Hester, D.A. Eisner, An estimate of the calcium content of the sarcoplasmic reticulum in rat ventricular myocytes, Pflugers Arch 423(1-2) (1993) 158-60.
[45] H.S. Choi, D.A. Eisner, The role of sarcolemmal Ca2+-ATPase in the regulation of resting calcium concentration in rat ventricular myocytes, J Physiol 515 (Pt 1)(Pt 1) (1999) 109-18.
[46] E. Dries, V. Bito, I. Lenaerts, G. Antoons, K.R. Sipido, N. Macquaide, Selective modulation of coupled ryanodine receptors during microdomain activation of calcium/calmodulin-dependent kinase II in the dyadic cleft, Circ Res 113(11) (2013) 1242-52.

[47] D. Baddeley, I.D. Jayasinghe, L. Lam, S. Rossberger, M.B. Cannell, C. Soeller, Optical single-channel resolution imaging of the ryanodine receptor distribution in rat cardiac myocytes, Proc Natl Acad Sci U S A 106(52) (2009) 22275-80.
[48] E. Dries, D.J. Santiago, D.M. Johnson, G. Gilbert, P. Holemans, S.M. Korte, H.L. Roderick, K.R. Sipido, Calcium/calmodulin-dependent kinase II and nitric oxide synthase 1-dependent modulation of ryanodine receptors during beta-adrenergic stimulation is restricted to the dyadic cleft, J Physiol 594(20) (2016) 5923-5939.
[49] N. Banterle, K.H. Bui, E.A. Lemke, M. Beck, Fourier ring correlation as a resolution criterion for super-resolution microscopy, J Struct Biol 183(3) (2013) 363-367.
[50] C. Soeller, D. Baddeley, Super-resolution imaging of EC coupling protein distribution in the heart, J Mol Cell Cardiol 58 (2013) 32-40.
[51] M.B. Cannell, C.H.T. Kong, M.S. Imtiaz, D.R. Laver, Control of Sarcoplasmic Reticulum Ca2+ Release by Stochastic RyR Gating within a 3D Model of the Cardiac Dyad and Importance of Induction Decay for CICR Termination, Biophys J 104(10) (2013) 2149-2159.
[52] J. Chung, A. Tilunaite, D. Ladd, H. Hunt, C. Soeller, E.J. Crampin, S.T. Johnston, H.L. Roderick, V. Rajagopal, IP(3)R activity increases propensity of RyR-mediated sparks by elevating dyadic [Ca(2＋)], Math Biosci 355 (2023) 108923.
[53] M.A. Walker, G.S.B. Williams, T. Kohl, S.E. Lehnart, M.S. Jafri, J.L. Greenstein, W.J. Lederer, R.L. Winslow, Superresolution modeling of calcium release in the heart, Biophys J 107(12) (2014) 3018-3029.
[54] M.B. Cannell, C.H. Kong, M.S. Imtiaz, D.R. Laver, Control of sarcoplasmic reticulum Ca2+ release by stochastic RyR gating within a 3D model of the cardiac dyad and importance of induction decay for CICR termination, Biophys J 104(10) (2013) 2149-59.
[55] K. Acsai, G. Antoons, L. Livshitz, Y. Rudy, K.R. Sipido, Microdomain [Ca(2)(+)] near ryanodine receptors as reported by L-type Ca(2)(+) and Na+/Ca(2)(+) exchange currents, J Physiol 589(Pt 10) (2011) 2569-83.
[56] T. Schendel, R. Thul, J. Sneyd, M. Falcke, How does the ryanodine receptor in the ventricular myocyte wake up: by a single or by multiple open L-type Ca2+ channels?, Eur Biophys J 41(1) (2012) 27-39.
[57] P. De Smet, J.B. Parys, G. Callewaert, A.F. Weidema, E. Hill, H. De Smedt, C. Erneux, V. Sorrentino, L. Missiaen, Xestospongin C is an equally potent inhibitor of the inositol 1,4,5-trisphosphate receptor and the endoplasmic-reticulum Ca(2+) pumps, Cell Calcium 26(1-2) (1999) 9-13.
[58] I. Smyrnias, N. Goodwin, D. Wachten, J. Skogestad, J.M. Aronsen, E.L. Robinson, K. Demydenko, A. Segonds-Pichon, D. Oxley, S. Sadayappan, K. Sipido, M.D. Bootman, H.L. Roderick, Contractile responses to endothelin-1 are regulated by PKC phosphorylation of cardiac myosin binding protein-C in rat ventricular myocytes, J Mol Cell Cardiol 117 (2018) 1-18.
[59] J. Mayourian, D.K. Ceholski, D.M. Gonzalez, T.J. Cashman, S. Sahoo, R.J. Hajjar, K.D. Costa, Physiologic, Pathologic, and Therapeutic Paracrine Modulation of Cardiac Excitation-Contraction Coupling, Circ Res 122(1) (2018) 167-183.
[60] H. Nakayama, I. Bodi, M. Maillet, J. DeSantiago, T.L. Domeier, K. Mikoshiba, J.N. Lorenz, L.A. Blatter, D.M. Bers, J.D. Molkentin, The IP3 receptor regulates cardiac hypertrophy in response to select stimuli, Circ Res 107(5) (2010) 659-66.
[61] A.L. Escobar, C.G. Perez, M.E. Reyes, S.G. Lucero, D. Kornyeyev, R. Mejia-Alvarez, J. Ramos-Franco, Role of inositol 1,4,5-trisphosphate in the regulation of ventricular Ca(2+) signaling in intact mouse heart, J Mol Cell Cardiol 53(6) (2012) 768-79.
[62] W.E. Louch, V. Bito, F.R. Heinzel, R. Macianskiene, J. Vanhaecke, W. Flameng, K. Mubagwa, K.R. Sipido, Reduced synchrony of Ca2+ release with loss of T-tubules-a comparison to Ca2+ release in human failing cardiomyocytes, Cardiovasc Res 62(1) (2004) 63-73.

[63] L.S. Song, S.Q. Wang, R.P. Xiao, H. Spurgeon, E.G. Lakatta, H. Cheng, beta-Adrenergic stimulation synchronizes intracellular Ca(2+) release during excitation-contraction coupling in cardiac myocytes, Circ Res 88(8) (2001) 794-801.
[64] I.S.J. Blanch, M. Egger, Obstruction of ventricular Ca(2+) -dependent arrhythmogenicity by inositol 1,4,5-trisphosphate-triggered sarcoplasmic reticulum Ca(2+) release, J Physiol 596(18) (2018) 4323-4340.
[65] F. Hohendanner, S. Walther, J.T. Maxwell, S. Kettlewell, S. Awad, G.L. Smith, V.A. Lonchyna, L.A. Blatter, Inositol-1,4,5-trisphosphate induced Ca2+ release and excitation-contraction coupling in atrial myocytes from normal and failing hearts, J Physiol 593(6) (2015) 1459-77.
[66] P.J. Mohler, J.Q. Davis, V. Bennett, Ankyrin-B coordinates the Na/K ATPase, Na/Ca exchanger, and InsP3 receptor in a cardiac T-tubule/SR microdomain, PLoS Biol 3(12) (2005) e423.
[67] F.M. Drawnel, D. Wachten, J.D. Molkentin, M. Maillet, J.M. Aronsen, F. Swift, I. Sjaastad, N. Liu, D. Catalucci, K. Mikoshiba, C. Hisatsune, H. Okkenhaug, S.R. Andrews, M.D. Bootman, H.L. Roderick, Mutual antagonism between IP3RII and miRNA-133a regulates calcium signals and cardiac hypertrophy., J Cell Biol 199(5) (2012) 783-798.
[68] X. Shen, J. van den Brink, Y. Hou, D. Colli, C. Le, T.R. Kolstad, N. MacQuaide, C.R. Carlson, P.M. Kekenes-Huskey, A.G. Edwards, C. Soeller, W.E. Louch, 3D dSTORM imaging reveals novel detail of ryanodine receptor localization in rat cardiac myocytes, J Physiol 597(2) (2019) 399-418.
[69] S. Galice, Y. Xie, Y. Yang, D. Sato, D.M. Bers, Size Matters: Ryanodine Receptor Cluster Size Affects Arrhythmogenic Sarcoplasmic Reticulum Calcium Release, J Am Heart Assoc 7(13) (2018).
[70] N. Macquaide, H.T. Tuan, J. Hotta, W. Sempels, I. Lenaerts, P. Holemans, J. Hofkens, M.S. Jafri, R. Willems, K.R. Sipido, Ryanodine receptor cluster fragmentation and redistribution in persistent atrial fibrillation enhance calcium release, Cardiovasc Res 108(3) (2015) 387-98.
[71] D.J. Bare, C.S. Kettlun, M. Liang, D.M. Bers, G.A. Mignery, Cardiac type 2 inositol 1,4,5-trisphosphate receptor: interaction and modulation by calcium/calmodulin-dependent protein kinase II, J Biol Chem 280(16) (2005) 15912-20.
[72] P.D. Swaminathan, A. Purohit, T.J. Hund, M.E. Anderson, Calmodulin-dependent protein kinase II: linking heart failure and arrhythmias, Circ Res 110(12) (2012) 1661-77.
[73] J. Curran, K.H. Brown, D.J. Santiago, S. Pogwizd, D.M. Bers, T.R. Shannon, Spontaneous Ca waves in ventricular myocytes from failing hearts depend on Ca(2+)-calmodulin-dependent protein kinase II, J Mol Cell Cardiol 49(1) (2010) 25-32.
[74] Y.H. Zhang, J.C. Hancox, Regulation of cardiac Na+-Ca2+ exchanger activity by protein kinase phosphorylation--still a paradox?, Cell Calcium 45(1) (2009) 1-10.
[75] R. Fischer, R. Dechend, A. Gapelyuk, E. Shagdarsuren, K. Gruner, A. Gruner, P. Gratze, F. Qadri, M. Wellner, A. Fiebeler, R. Dietz, F.C. Luft, D.N. Muller, A. Schirdewan, Angiotensin II-induced sudden arrhythmic death and electrical remodeling, Am J Physiol Heart Circ Physiol 293(2) (2007) H1242-53.
[76] S. Garg, J. Narula, C. Marelli, D. Cesario, Role of angiotensin receptor blockers in the prevention and treatment of arrhythmias, Am J Cardiol 97(6) (2006) 921-5.

Methods

Animal model

A porcine model of myocardial remodelling after myocardial infarction (MI) and chronic ischemia as described previously was used [46]. Presence of infarct and expected alterations in hemodynamics properties determined by MRI are presented in Table S1. Animals were housed and treated according to the European Directive 2010/63/EU with protocols approved by the local ethical committee (Ethische Commissie Dierproeven, KU Leuven).

General Methods

Detailed reagents, methods for CM isolation, Ca^{2+} imaging with electrophysiology, immunoblotting, DNA-PAINT microscopy, RT-qPCR, mathematical modelling and statistical analysis are provided in the Extended Methods and in [39, 46, 48].

Graphical Abstract: Mechanism underlying pro-arrhythmic action of $InsP_3$-induced Ca^{2+} release. Remodelling of cardiomyocyte TT and $InsP_3R$ expression in healthy and post-MI heart is shown. **A.** in healthy heart, $InsP_3R$ expression is low, and electrical stimulation (black arroes) induces Ca^{2+} entry via LTCC that activate Ca^{2+} release via RyRs on coupled dyads to generate a Ca^{2+} transient. **B.** In MI, TT are lost leading to increased non coupled RyRs and slower CaT are observed. $InsP_3Rs$ expression is also increased. **C.** As in B but in the presence of increased $InsP_3$, Ca^{2+} release via RyRs, including non coupled RyRs, is increased leading to augmented Ca^{2+} transient kinetics and Ca^{2+} waves, which engage NCX, and if of sufficient magnitude, reach threshold for AP generation. Smaller Ca^{2+} waves produce DADs.

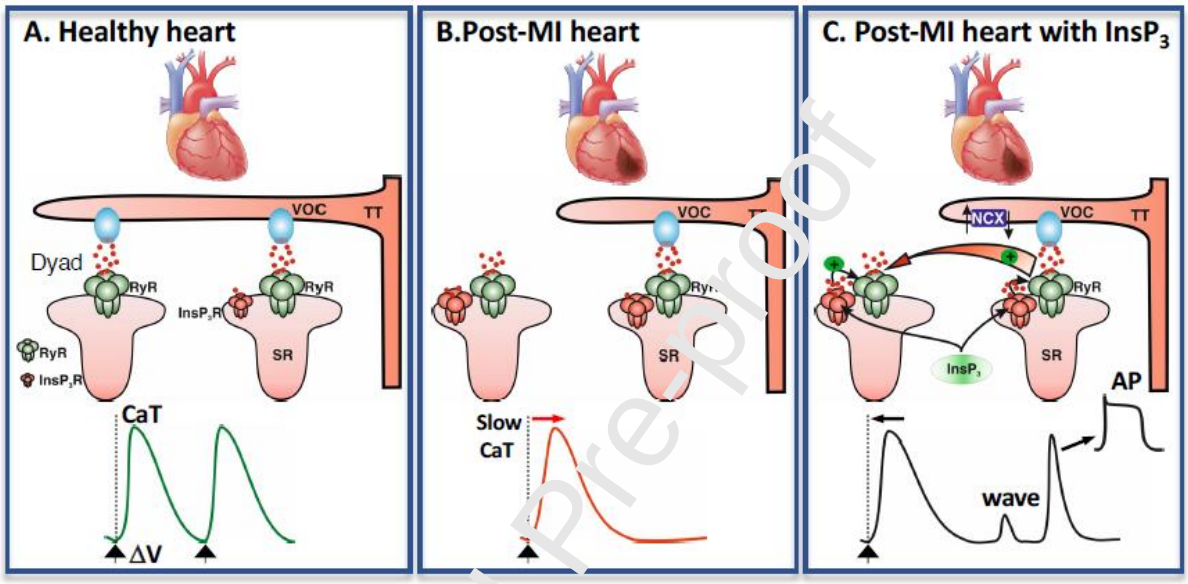

Highlights:

- $InsP_3R$ expression is upregulated in a pig model of ischemic heart disease.
- $InsP_3$ increases Ca^{2+} sparks via RyR in post-MI pig cardiomyocytes.
- Ca^{2+} release via $InsP_3Rs$ induces arrhythmogenic activity in MI pig cardiomyocytes.
- Nanoscale imaging reveals co-habitation of $InsP_3Rs$ and RyRs within clusters.
- Mathematical modeling supports role for $InsP_3Rs$ in RyR cluster activation in ECC.